AGU ADVANCING EARTH AND SPACE SCIENCE

Water Resources Research

RESEARCH ARTICLE
10.1029/2020WR028962

Modeling Decadal Salt Marsh Development: Variability of the Salt Marsh Edge Under Influence of Waves and Sediment Availability

P. W. J. M. Willemsen[1,2,3], B. P. Smits[3], B. W. Borsje[1], P. M. J. Herman[3,4], J. T. Dijkstra[3], T. J. Bouma[2], and S. J. M. H. Hulscher[1]

[1]Water Engineering & Management, University of Twente, Enschede, The Netherlands, [2]Department of Estuarine and Delta Systems, NIOZ Royal Netherlands Institute for Sea Research and Utrecht University, Yerseke, The Netherlands, [3]Department of Ecosystems and Sediment Dynamics, Deltares, Delft, The Netherlands, [4]Faculty of Civil Engineering and Geosciences, Delft University of Technology, Delft, The Netherlands

Key Points:

- 50-year biogeomorphological development of salt marshes, forced by waves and suspended sediment, is modeled
- Seaward extension is observed with low wave forcing, whereas landward retreat is observed with high wave forcing
- Salt marshes forced with high waves are able to switch from a retreating to an expanding extent, with increasing sediment availability

Correspondence to:
P. W. J. M. Willemsen,
p.willemsen@utwente.nl

Citation:
Willemsen, P. W. J. M., Smits, B. P., Borsje, B. W., Herman, P. M. J., Dijkstra, J. T., Bouma, T. J., & Hulscher, S. J. M. H. (2022). Modeling decadal salt marsh development: Variability of the salt marsh edge under influence of waves and sediment availability. *Water Resources Research*, *58*, e2020WR028962. https://doi.org/10.1029/2020WR028962

Received 7 NOV 2020
Accepted 18 DEC 2021

Author Contributions:
Conceptualization: P. W. J. M. Willemsen, B. W. Borsje, P. M. J. Herman, J. T. Dijkstra
Formal analysis: P. W. J. M. Willemsen, B. P. Smits
Funding acquisition: T. J. Bouma, S. J. M. H. Hulscher
Investigation: P. W. J. M. Willemsen
Methodology: P. W. J. M. Willemsen, B. P. Smits, P. M. J. Herman, J. T. Dijkstra
Project Administration: B. W. Borsje, T. J. Bouma, S. J. M. H. Hulscher
Resources: P. W. J. M. Willemsen, B. W. Borsje, J. T. Dijkstra
Software: P. W. J. M. Willemsen, B. P. Smits
Supervision: B. W. Borsje, T. J. Bouma, S. J. M. H. Hulscher

Abstract Salt marshes can contribute to coastal protection, but the magnitude of the protection depends on the width of the marsh. The cross-shore width of the marsh is to a large extent determined by the delicate balance between seaward expansion and landward retreat. The influence of the magnitude of daily occurring mild weather conditions and sediment availability on the variability of salt marsh width has not been systematically assessed. This paper investigates how the magnitude of homogeneous hydrodynamic forcing, combined with sediment availability, affects the biophysical development, and more specifically retreat and expansion of salt marshes. The dynamic extent of the salt marsh is assessed by modeling online-coupled hydrodynamics, morphodynamics and vegetation growth using the numerical Delft3D-Flexible Mesh model, and a vegetation growth module. Simulated patterns around the salt marsh edge resembled field observations, as well as the simulated temporal variability of the lateral position of the salt marsh edge. In the model, the salt marsh extended seaward at low wave forcing (0.00 m; 0.05 m), and retreated landward at higher wave forcing (0.10 m; 0.15 m). With increasing physical stress, the salt marsh edge was found at lower elevations, indicating an unhealthy system with a retreating marsh edge due to vegetation mortality, whereas decreasing physical stresses result in a higher salt marsh edge, enabling expansion. This balance suggests the importance of response time of vegetation to physical stress. Yet, the salt marsh forced with higher waves was able to switch from a retreating extent retrogradational to an expansional behavior as sediment supply increased.

1. Introduction

Salt marshes are able to stabilize the coast by attenuating wave energy and can increase the bed level by trapping sediment and accumulation of organic matter (Bouma et al., 2005; Kirwan & Megonigal, 2013; Kirwan et al., 2016; Mudd et al., 2009; Turner et al., 2004). In the last decades, the stabilizing character of salt marshes and their wave attenuating capacity has led to an increasing interest in incorporating them in coastal protection (Borsje et al., 2011; Gedan et al., 2011; King & Lester, 1995; Shepard et al., 2011; Temmerman et al., 2013; Vuik et al., 2019). A recent historic analysis reveals that marshes have significantly contributed to flood safety in the past, with marsh width being a key parameter for their flood defense value (Zhu, Vuik et al., 2020). Salt marshes can very well withstand the short-term stress of storm conditions and keep their wave attenuation capacity during storms, as has been demonstrated in large-scale flume experiments (Möller et al., 2014), in the field (Kirwan & Megonigal, 2013; Kirwan et al., 2016; Vuik et al., 2016) and in combined field and model studies (Willemsen et al., 2020).

Climate change is expected to modify the environmental conditions along the coast, primarily through increased Sea Level Rise (SLR), and also through the prevalence of storms, which are predicted to be more severe and more frequent in the future (Emanuel, 2005; Knutson et al., 2010; Kolker et al., 2009; Leckebusch & Ulbrich, 2004). In contrast to conventional coastal protection, salt marshes have better abilities to cope with climate change effects by adapting to changing environmental conditions (Borsje et al., 2011).

The interaction between the vegetation, hydrodynamics and sediment dynamics plays a key role in all of these adaptations (Bouma et al., 2016; Willemsen et al., 2018). Plants need minimum growth rates to withstand the different stressors of the physically demanding saltmarsh habitat (Balke et al., 2013). A trade-off exists between

Validation: P. W. J. M. Willemsen, B. W. Borsje
Visualization: P. W. J. M. Willemsen, B. W. Borsje
Writing – original draft: P. W. J. M. Willemsen, B. P. Smits, B. W. Borsje
Writing – review & editing: P. W. J. M. Willemsen, B. W. Borsje, P. M. J. Herman, J. T. Dijkstra, T. J. Bouma, S. J. M. H. Hulscher

different forms of stress. As an example, for vegetation to establish at low locations with long inundation stress, bed levels need to be very stable. Conversely, establishment of vegetation on dynamic beds will only be possible at lower inundation stress and thus higher elevation relative to mean sea level (Bouma et al., 2016; Willemsen et al., 2018). Lateral dynamics of the marsh edge are driven by two phases, lateral retreat (Leonardi et al., 2016; Mariotti & Fagherazzi, 2013) and expansion (Zhang et al., 2004; Zhang et al., 2020; Zhang et al., 2011), that show cyclic alternations over time in many locations (Allen, 2000; Singh Chauhan, 2009; Van de Koppel et al., 2005; Van der Wal et al., 2008).

Lateral retreat can be initiated by cliff formation and/or vegetation mortality, which occurs if a marsh expands to far out on the tidal flat (Bouma et al., 2016). The retreat rate is driven by flooding frequency and continuously occurring normal weather conditions, causing marsh edges that are exposed to prevailing wind direction to retreat faster (Fagherazzi, 2014; Wang et al., 2017). Expansion is initiated by seedling establishment (Bouma et al., 2016) and subsequent growth of clonal shoots (Silinski et al., 2016).

Previous studies assessing retreat of the cliff, show a clear relation between wave power and cliff retreat (Bendoni et al., 2016; Leonardi & Fagherazzi, 2014; Leonardi et al., 2016; Marani et al., 2011; Zhao, Yu et al., 2017). Eroded sediments originating from the cliff can contribute to growth of vegetation in front of the cliff, thereby stimulating short-term expansion (Mariotti, 2020). Also more seaward from the cliff, pioneer vegetation is able to establish and colonize the tidal flat in absence of physical stress (Bouma et al., 2016; Pedersen & Bartholdy, 2007), highlighting that the cliff is not per definition equal to the vegetation edge.

Feedback mechanisms are fundamental for the vertical and lateral expansion and retreat of the salt marsh under different environmental conditions. Provided sufficient sediment is available to be trapped by the vegetation, salt marshes grow with SLR (e.g., Best et al., 2018; Kirwan et al., 2010; Kirwan et al., 2016). During storm events sediment supply toward the salt marsh increases, due to resuspension of sediment from the tidal flat and increased water levels over the marsh. This enhances vertical growth of salt marshes during storms (Kolker et al., 2009; Schuerch et al., 2013). Moreover, vegetation presence at the salt marsh edge might reduce wave-induced lateral erosion (Feagin et al., 2009; Wang et al., 2017). However, insufficient sediment availability inhibits marsh growth, increases wave energy hence promoting erosion (Mariotti & Fagherazzi, 2013). The positive effect of wind-driven waves on vertical accretion during extreme events, given sufficient sediment supply, contrasts with the lateral erosion at the marsh edge, caused by relatively small waves during continuous mild weather conditions (Callaghan et al., 2010; Fagherazzi, 2014; Tonelli et al., 2010).

Taking all effects into account, the lateral development of a salt marsh, that is, seaward expansion or landward retreat, depends on (a) the relative elevation to mean sea level (Mariotti & Fagherazzi, 2010; Temmerman et al., 2004), (b) the sediment supply (Ladd et al., 2019; Mariotti & Fagherazzi, 2010), (c) the wave climate (Leonardi et al., 2016; Marani et al., 2011), and obviously (d) the moment in the tidal phase (i.e., spring-neap) at which storms occur, which affects bed shear stresses due to waves. For the use of salt marshes in a hybrid coastal flood defense, a quantitative understanding of the dynamics of the cross-shore marsh width on decadal timescales is essential (Bouma et al., 2016).

The vertical growth of salt marshes, as influenced by sediment supply, wave climate and SLR, is well-studied (e.g., Schuerch et al., 2013; Temmerman et al., 2004). Also the retreat of the marsh edge by cliff erosion over a rather short timescale (snapshot to years) has been analyzed with coupled field observations and modeling studies (e.g., Bendoni et al., 2016; Tonelli et al., 2010). However, the effect of different levels of relatively mild wave conditions on decadal vegetation development at the seaward edge of the salt marsh has not been quantified. Previous studies did not systematically assess process-based vegetation dynamics around the seaward salt marsh edge. Moreover, the long-term biological development around the salt marsh edge, that is, vegetation patterns and development of vegetation density, affected by sediment availability and homogenous waves is not yet detailed described. To assess both seaward expansion and landward retreat of vegetation at the salt marsh edge in a single model, a detailed long-term process-based description of interaction between hydrodynamics, morphodynamics and a process-based vegetation development module is a prerequisite.

In this paper we aim to understand the cross-shore width of the vegetated salt marsh over a decadal time scale and yearly variability of this width by simulating retreat and expansion of the salt marsh due to homogeneous hydrodynamic forcing and sediment availability. Building on previous research (e.g., D'Alpaos et al., 2011; Kirwan et al., 2010; Temmerman et al., 2007), we explicitly combine a process-based vegetation growth module,

with hydrodynamic and morphodynamic development in a schematic biophysical setting. We hypothesize that (a) the variability of the marsh edge location defined by vegetation presence increases with wave height, because of continuous re-establishment of the eroding tidal flat, (b) until hydrodynamic stresses disable the opportunity for vegetation to establish. We will assess the dynamic lateral extent of the salt marsh schematically by modelling bed level change and vegetation growth over a period of 50 years in a two dimensional (depth-averaged) model. We will focus on vegetation dynamics at the salt marsh edge, thereby not aiming at a real world representation, but an understanding of the variability of the location of the salt marsh edge, given hydrodynamic forcing and sediment availability. The biophysical settings of the model are based on and compared with field observations of existing salt marshes in the Netherlands.

2. Methods

We developed an online-coupled model able to reproduce the feedbacks between hydrodynamics, morphodynamics and vegetation dynamics. Using this set-up, the role of homogeneous mild wave conditions, derived from daily weather conditions, and sediment availability derived from the locally occurring range, are systematically assessed.

2.1. Physical Settings of the Salt Marsh

Parameter settings and salt marsh characteristics were derived from salt marshes in the Westerschelde estuary (southwestern part of the Netherlands (Figure 1). The spring tidal range at the center of the Westerschelde (51° 23' N, 3° 50' E) is 4.93 m, with MHWN (mean high water neap) at 1.85 m + MSL (mean sea level) and MHWS (mean high water spring) at 2.63 m + MSL (Van der Wal et al., 2008; Willemsen et al., 2020). The salinity is approximately 20–25 psu (Damme et al., 2005). The northern shores are more exposed to the prevailing winds from the southwest than the sheltered southern shores (Callaghan et al., 2010). Vegetation species in the pioneer zone (lower marsh) are mostly the perennial common cord grass (*Spartina anglica*) and the annual glasswort (*Salicornia spp*.). Higher up in the marsh dominant species are common saltmarsh grass (*Puccinellia maritima*), annual seablite (*Suaeda maritima*), and sea aster (*Aster tripolium*) (Van der Wa et al., 2008).

Detailed bathymetric data in the intertidal zone of the Westerschelde are extensively available (De Kruif, 2001; Marijs & Parée, 2004; Wiegman et al., 2005). The initial bathymetry from the model was derived from decadal field observations of elevation data in a marsh on the northern shore (Zuidgors) and one on the southern shore (Paulinapolder) (Willemsen et al., 2020). The considered salt marshes contrast in wind exposure and development of the salt marsh edge. Zuidgors at the northern shores is exposed to the prevailing wind direction and the marsh edge is retreating, whereas Paulinapolder is sheltered from the prevailing wind direction and the marsh edge is expanding. Both salt marshes are located in a landward inflection of the dike, relatively sheltered from longshore currents (Figure 1). The data set from Willemsen et al. (2020), containing bathymetric profiles every 250 m alongshore for six salt marshes in the Westerschelde estuary, including Zuidgors and Paulinapolder, was used to compare field observations of the decadal dynamics of the salt marsh edge over the past 60 years (1955–2015) with model results (Section 3.3.3).

2.2. Biogeomorphological Model Description

2.2.1. Hydrodynamic and Morphodynamic Model

The Delft3D Flexible Mesh (Delft3D-FM) model was used in the current study to simulate hydrodynamics, sediment dynamics and morphological processes. This model and its predecessor Delft3D are widely used in coastal, estuarine and riverine systems (e.g., Achete et al., 2016; Kernkamp et al., 2011; Ruessink & Roelvink, 2000). The unsteady shallow water equations in the flow module D-Flow FM (Flexible Mesh) are solved two dimensionally (depth-averaged) (Appendix A).

D-Waves was used to simulate waves (Deltares, 2019c). D-Waves is based on the third generation Simulating WAves Nearshore (SWAN) spectral wave model (Booij et al., 1999; Ris et al., 1999). D-Waves can be used to simulate the evolution of random, short-crested wind-generated waves in coastal regions. The model computes wave propagation, wave generation by wind, non-linear wave-wave interaction and dissipation (Appendix A).

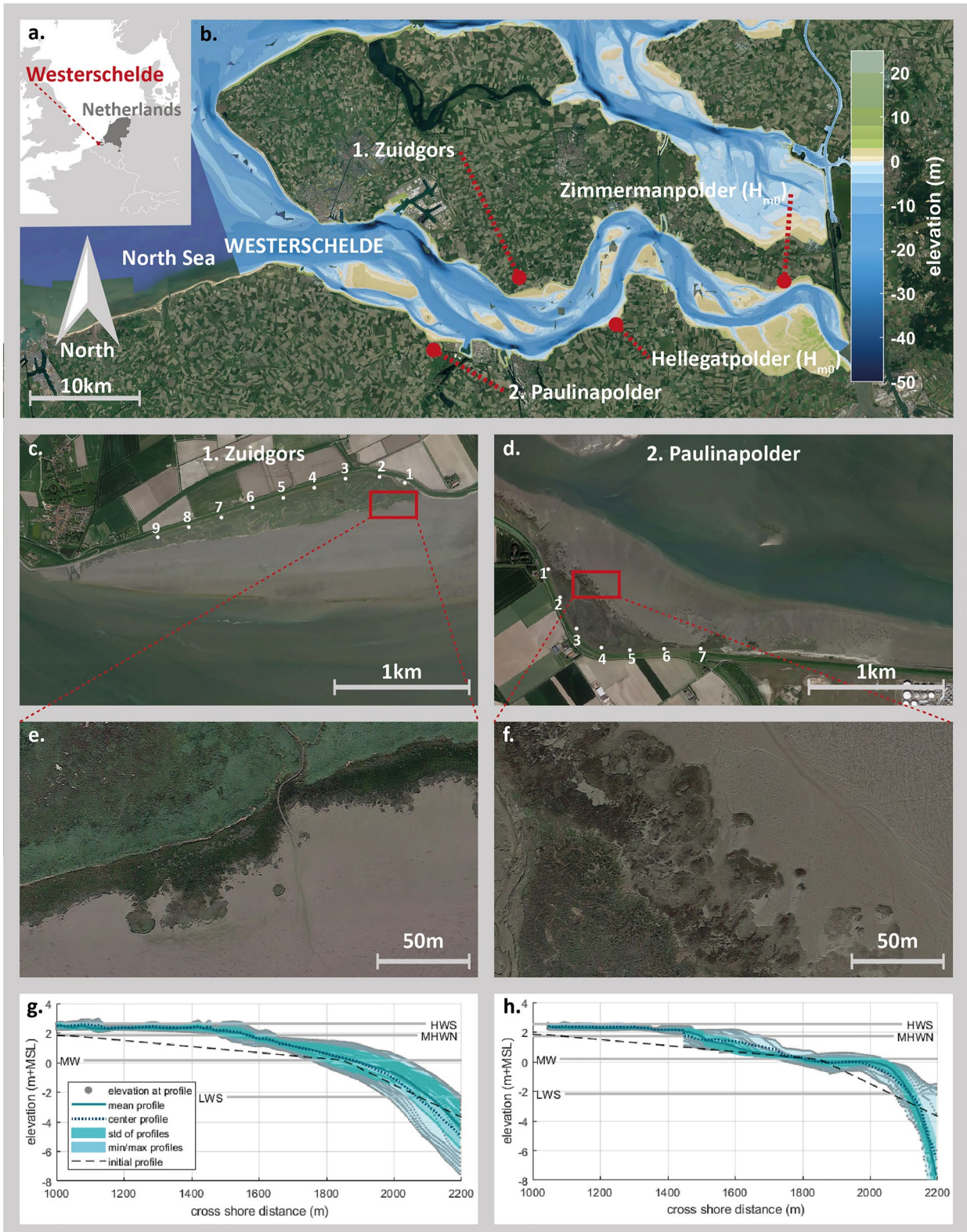

Figure 1. (a) The Westerschelde estuary in the Netherlands. (b) The overlay shows the bathymetry from 2015. Two salt marshes located in the center of the estuary, that is, Zuidgors (a, e, g) and Paulinapolder (d, f, h) were used to determine parameter settings for the model. An aerial picture highlights the salt marsh and fronting tidal flat (c and d), with a zoom on the vegetation edge (e and f). The white dots highlight the starting points of the transects used to derive the variability of the salt marsh edge (c and d). Profiles of both study sites were used to determine the initial profile in the model (g and h). Source aerial imagery: Google Earth.

Transport of cohesive sediment was calculated using D-Morphology (Deltares, 2019b) by solving the advection-diffusion equation for suspended sediment, whilst sedimentation and erosion are calculated with the Partheniades-Krone equations (Partheniades, 1965) (Appendix A).

Shear stresses exerted by vegetation on the flow were taken into account by using the trachytopes model in D-Flow FM (Deltares, 2019a). The flow resistance is parameterized by means of a bed roughness determined by plant dimensions following Baptist (2005). To mitigate excessive bed shear stresses, an additional term representing the flow resistance of the vegetation is included in the momentum equation too (Deltares, 2019a). Wave attenuation by vegetation is resolved by the Méndez-Losada equation (Méndez & Losada, 2004; Suzuki et al., 2012) (Appendix A).

2.2.2. Dynamic Vegetation Model

Vegetation establishment and growth for *Spartina anglica* was calculated by the population dynamics balance equation (Equation 1) (Schwarz et al., 2014; Temmerman et al., 2007). The change of the total stem density over time was calculated as a result of vegetation establishment (Equation 2), lateral expansion of plants through diffusion to neighboring cells (Equation 3), clonal growth of plants up to the maximum carrying capacity by using a logistic function (Equation 4), plant mortality caused by shear stress due to flow and waves (Equation 5) and plant mortality due to inundation stress, proportional to inundation height at high tide (Equation 6).

$$\frac{\partial n_b}{\partial t} = \left(\frac{\partial n_b}{\partial t}\right)_{\text{est}} + \left(\frac{\partial n_b}{\partial t}\right)_{\text{diff}} + \left(\frac{\partial n_b}{\partial t}\right)_{\text{growth}} - \left(\frac{\partial n_b}{\partial t}\right)_{\text{flowwave}} - \left(\frac{\partial n_b}{\partial t}\right)_{\text{inund}} \tag{1}$$

$$\left(\frac{\partial n_b}{\partial t}\right)_{\text{est}} = r_{01}(P_{\text{est}}) * n_{b,0} \tag{2}$$

$$\left(\frac{\partial n_b}{\partial t}\right)_{\text{diff}} = D\left(\frac{\partial^2 n_b}{\partial x^2} + \frac{\partial^2 n_b}{\partial y^2}\right) \tag{3}$$

$$\left(\frac{\partial n_b}{\partial t}\right)_{\text{growth}} = r * \left(1 - \frac{n_b}{K}\right) n_b \tag{4}$$

$$\left(\frac{\partial n_b}{\partial t}\right)_{\text{flowwave}} = -n_b * C_{\text{tau}} * (\tau - \tau_{\text{cr},p}), \quad \text{when} \quad \tau > \tau_{\text{cr},p} \tag{5}$$

$$\left(\frac{\partial n_b}{\partial t}\right)_{\text{inund}} = -n_b * C_{\text{inund}} * (H - H_{\text{cr},p}), \quad \text{when} \quad H > H_{\text{cr},p} \tag{6}$$

where $\partial n_b/\partial t$ represents the change of the stem density per cell over time [stems $m^{-2}d^{-1}$]. $r_{01}(P_{\text{est}})$ is a function generating at random either a 0 (with probability $1 - P_{\text{est}}$) or a 1 (with probability P_{est}). The random numbers were generated independently per time step and per cell in the model domain. $n_{b,0}$ is the initial stem density [m^{-2}], D is the plant diffusion coefficient [m^2 yr^{-1}], x and y are the horizontal spatial coordinates [m], r is the intrinsic growth rate of the stem density [d^{-1}], K is the maximum carrying capacity of the stem density [m^{-2}], C_{tau} is the plant mortality coefficient due to bed shear stress [d^{-1} ($N\ m^{-2}$)$^{-1}$], τ is the bed shear stress exerted by flow and waves [$N\ m^{-2}$], $\tau_{\text{cr},p}$ is the critical bed shear stress for plant mortality [$N\ m^{-2}$], C_{inund} is the plant mortality coefficient due to inundation stress [$d^{-1}\ m^{-1}$], H is the inundation height [m], and $H_{\text{cr},p}$ is the critical inundation height at high tide [m].

2.2.3. Biogeomorphological Coupling

The vegetation growth module was set up in Python. This module was coupled to the hydrodynamic (both flow and wave) and the morphological Delft3D-FM model through BMI (Basic Model Interface) (Hutton et al., 2020; Peckham et al., 2013) (Figure 2). BMI exchanges memory location pointers between the Delft3D-FM and Python models. Consequently, model parameters and (state) variables are exchanged through memory, thus avoiding any file writing and reading when switching between the codes. The flow model simulates tidal flow with a computational time step of maximum 30 s; this timestep decreases if the maximum Courant number of 0.7 is exceeded (Deltares, 2019a). The wave model was set up to simulate wave propagation every 3600 s.

Morphological change was calculated every computational timestep ('online'). However, the morphological change was multiplied with an acceleration factor ('MorFac'; Roelvink, 2006) of 100 every single timestep. The

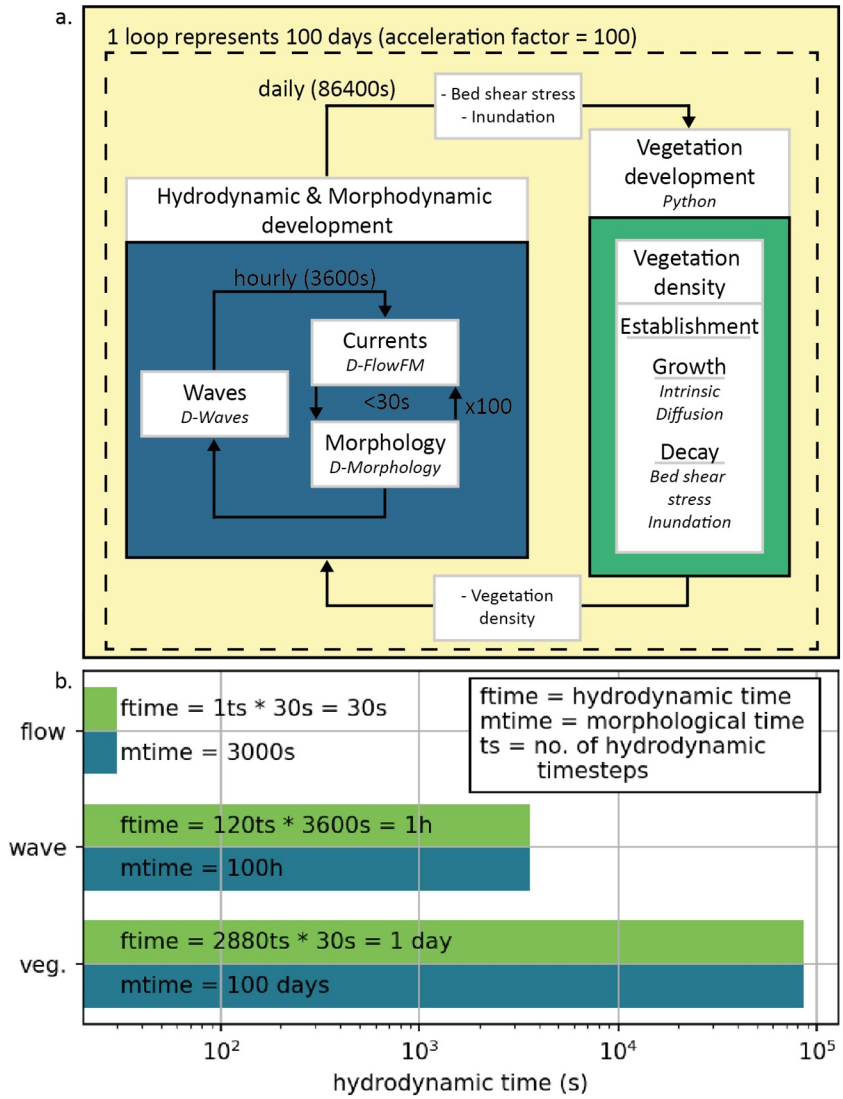

Figure 2. (a) Flowchart of modeling approach and online coupling of interactive computation of hydrodynamic, morphodynamic and vegetation development using the Basic Model Interface (BMI). (b) Hydrodynamic and morphodynamic time for the hydrodynamic models and vegetation model with an morphological acceleration factor of 100.

computation of a subsequent hydrodynamic timestep uses the morphological change multiplied by the acceleration factor, ensuring that the hydrodynamic computations are carried out using the correct bathymetry. Applying this factor means that 3.6 days of hydrodynamic calculations represents the morphological change of a single year, that is, 180 hydrodynamic days represent 50 years. A full spring-neap cycle of approximately 14 days represents the morphological change of 3.9 years. The acceleration factor used in this study was equal to the acceleration factor used in Best et al. (2018), whereas earlier studies of salt marsh development used an acceleration factor of approximately 700 (Temmerman et al., 2007). The vegetation development was calculated once every 100 morphodynamic days (i.e., once every single hydrodynamic day); the change in vegetation over a time step of nominally one day, corresponds to vegetation change over 100 days in the morphological timescale. This is assumed to be suitable for simulating yearly to decadal marsh width dynamics, forced with constant hydrodynamics and sediment dynamics. Moreover, vegetation dynamics was modeled as a year-averaged process, consequently seasonal variability was not included (Temmerman et al., 2007), even though several vegetation time steps occur in a single morphological year. The physical variables driving vegetation development (e.g., inundation height and bed shear stress), were cumulatively stored every hydrodynamic computational timestep (of maximum 30 s), for calculating vegetation dynamics.

The full model was controlled in Python. First, the vegetation establishment was calculated over the model grid. Next, the flow and morphodynamic model were executed every 30 s and the wave model every 3600 s over the vegetation timestep, which is 86.400 s (i.e., a hydrodynamic day equal to 100 days of morphodynamics and vegetation development) (Figure 2). After a day, hydrodynamic results over the vegetation time step were used to inform the vegetation growth and decay. In addition, new vegetation establishment was calculated. The results of the vegetation model, that is, new vegetation presence and density (plant dimensions were considered constant), were used to set a new vegetation roughness field in Delft3D-FM. Then a new loop of hydrodynamic and morphodynamic calculations started (Figure 2).

2.3. Model Setup

2.3.1. Model Domain

The model domain of the depth-averaged flow model represented an area with a cross-shore width of 2500 m and an alongshore length of 1000 m. The cell size applied over the full domain is 5 m, both in *x*- and *y*-direction. The domain of the wave model was larger in the alongshore direction (i.e., 2000 m) to prevent boundary effects. The cell size over the outer wave domain was 15 m, both in *x*- and *y*-direction. A grid with a smaller cell size was nested in the larger wave model, the alongshore length of the inner grid is 1100 m with a cell size of 5 m both in *x*- and *y*-direction.

2.3.2. Topography

A typical initial profile was derived from the data set presented in Willemsen et al. (2020). The direction of the profiles was approximately aligned to the wind direction during extreme events statistically occurring once every 10–10,000 years (Willemsen et al., 2020) (Figure 1), to be able to compare the simulated dynamics of the salt marsh edge with field observations and discuss Nature-Based Flood Defenses (NBFD) which are typically designed for extreme events with longer return periods. Relative to MSL, the initial bed level height at the most seaward location of the domain is −7 m, well below mean low water spring (MLWS) of −2.31 m (Zuidgors) and −2.16 m (Paulina). The bed level increased to the local mean sea level (0.16 m at Zuidgors; 0.19 m at Paulinapolder) over a distance of approximately 650 m. Subsequently the bed level reached MHWN, which is 1.85 m at Zuidgors and 1.73 m at Paulina, over a distance of 800 m (Figures 1g and 1h). This part of the profile was explicitly chosen to be linear, to prevent imposing a convex-up or concave-up profile affecting vegetation establishment and growth at the tidal flat and potential marsh area. MHWN has been used previously as fixed elevation threshold for vegetation growth in the Westerschelde (Doody, 2007; Van der Wal et al., 2008). Finally, the topography increased to mean high water spring (MHWS; 2.63 m at Zuidgors; 2.54 m at Paulina) over the last 1050 m of the domain. The initial topography was uniform in alongshore direction. Random perturbations in the range of –1 cm – +1 cm were added on to the initial bed elevation of each grid cell for initiation of pattern development (c.f. Best et al., 2018).

2.3.3. Boundary Conditions and Model Parameters

The model contained a single open boundary at the southern end of the model extent. The water levels at the open boundary were constructed using the semidiurnal M2 and S2 tidal constituents, resulting in a repeated spring-neap tidal cycle. The range of the tidal signal was 4.93 m with a mean tide level of 0.16 m (Van der Wal et al., 2008). MLWS and MHWS were −2.32 and 2.64 m respectively and MLWN and MHWN were −1.52 and 1.85 m respectively. Wave forcing was applied to the model by continuously imposing a mild wave height and wave period at the open southern boundary. The wave height at the boundary was based on measurements of the wave height seaward of the vegetation edge at a marsh at the northern and southern shores of the Westerschelde (Hellegatpolder and Zimmermanpolder resp.; Figure 1). The average wave height measured over approximately a year at both locations was approximately 0.11 m with a standard deviation of 0.07–0.08 m (Willemsen et al., 2018). The continuous wave heights used in the model scenarios were situated around this average. A directional spreading of 30° was applied. Suspended sediment concentrations (SSC) measured in the stream channel of the Westerschelde generally ranged between approximately 10 and 75 mg/L (10th and 90th percentile) (Temmerman et al., 2004; Van Damme et al., 1999). In the current model the vertically averaged suspended sediment concentration was

Table 1
Hydrodynamic, Sediment and Vegetation Growth Parameters Used in the Model Study

Parameter	Symbol	Value	Unit	Source
Uniform friction coefficient	N	0.023	s $m^{-1/3}$	Wamsley et al. (2010), Deltares (2019a)
Eddy viscosity	N	10	m^2 s^{-1}	Deltares (2015)
Eddy diffusivity	D	10	m^2 s^{-1}	Deltares (2015)
Reference density	$\rho_{s,0}$	1600	kg m^3	Best et al. (2018), Deltares (2019b)
Specific density	ρ_s	2,650	kg m^3	Best et al. (2018), Deltares (2019b)
Dry bed density	$\rho_{s,\mathrm{dry}}$	500	kg m^3	Best et al. (2018), Deltares (2019b)
Settling velocity cohesive sediment	ω_s	0.5	mm s^{-1}	Willemsen et al. (2018)
Critical bed shear stress for erosion	$\tau_{\mathrm{cr},e}$	0.5	N m^{-2}	Best et al. (2018), Deltares (2019b)
Critical bed shear stress for deposition	$\tau_{\mathrm{cr},d}$	1,000	N m^{-2}	Best et al. (2018), Deltares (2019b)
Erosion parameter	M	$5 * 10^{-5}$	kg m^{-2} s^{-1}	Best et al. (2018), Deltares (2019b)
Acceleration factor	AF	100	-	-
Chance of vegetation establishment	P_{est}	0.01		Schwarz et al. (2018)
Initial vegetation density of established vegetation	$n_{b,0}$	200	m^{-2} day^{-1}	van Hulzen et al. (2007)
Intrinsic growth rate of vegetation	R	1	Day^{-1}	van Hulzen et al. (2007)
Maximum carrying capacity of stem density	K	1,200	Stems m^{-2}	Temmerman et al. (2005)
Vegetation diffusion coefficient	D	0.2	m^2 day^{-1}	van Hulzen et al. (2007)
Vegetation mortality coefficient due to bed shear stress	C_{tau}	30	Day^{-1} $(N\ m^{-2})^{-1}$	van Hulzen et al. (2007)
Critical bed shear stress for vegetation mortality	$\tau_{\mathrm{cr},p}$	0.26	N m^{-2}	van Hulzen et al. (2007)
Vegetation mortality coefficient due to inundation stress	C_{inund}	3,000	Day^{-1} m^{-1}	van Hulzen et al. (2007)
Critical inundation height for vegetation mortality	$H_{\mathrm{cr},p}$	1.1	m	van Hulzen et al. (2007)
Uniform vegetation diameter	b_{veg}	0.0043	m	Temmerman et al. (2005)
Uniform vegetation height	h_{veg}	0.5	m	Temmerman et al. (2005)

Note. The vegetation time steps are defined in hydrodynamic days, equal to 100 morphodynamic days.

varied between 10 and 50 mg/L at the southern open boundary. Eroded sediment resuspended within the domain was re-allocated within the domain or flowed out via the open southern boundary.

2.3.4. Hydrodynamic Model Parameters

A uniform Manning bed roughness of 0.023 s $m^{-1/3}$ was used, which is slightly higher than the value for open waters (Wamsley et al., 2010), because of the location in the intertidal (Table 1). Manning values were comparable with values used in previous studies on salt marshes in general and salt marshes in the Westerschelde (e.g., Best et al., 2018). The horizontal eddy viscosity and eddy diffusivity should be typically in the range of 1–10 m^2 s for grid cell dimensions of tens of meters or less and were both set to 10 m^2 s, which is the default value (Deltares, 2015).

2.3.5. Morphodynamic Model Parameters

A uniform fine cohesive sediment was applied in the model, generally appearing at tidal flats and salt marshes in the Westerschelde (Willemsen et al., 2018). Default values were used for the reference density, specific density and dry bed density of the sediment, respectively 1600, 2650 and 500 kg m^{-3} (Table 1). The settling velocity for cohesive sediment was set to 0.5 mm s^{-1}, which is approximately the settling velocity of the average grain size diameter found around the salt marsh edge in the Westerschelde (Willemsen et al., 2018). A value of 0.5 N m^{-2} was applied for the critical bed shear stress for erosion, whereas the critical bed shear stress for deposition was set to 1000 N m^{-2} enabling sedimentation unrestricted by bed shear stresses. The erosion parameter was set to $5 * 10^{-5}$ kg m^{-2} s^{-1} (Best et al., 2018; Deltares, 2019b). To decrease the computational time an acceleration factor of 100 was applied (Figure 2).

2.3.6. Vegetation Growth and Decay

Vegetation growth was simulated by changing the stem density according to the population dynamics model. In this study the salt marsh species *Spartina anglica* (cordgrass) was simulated. The drag coefficient (C_D) of vegetation depends on hydrodynamic conditions and the vegetation species (Table 1). The drag coefficient under storm conditions for *Spartina anglica* was previously calibrated to be 0.5 (Vuik et al., 2016). Under small wave heights it can be assumed that the stems are rigid, for which a C_D coefficient of 1.0 is commonly used (Suzuki & Arikawa, 2010; van Veelen et al., 2020). In the current study a value of 0.7, in between the previous values, was used, to take into account various conditions and vegetation of different ages. Average values were assumed for the stem height (0.5 m) and stem thickness (4.3 mm) (Temmerman et al., 2007), whereas the vegetation density was variable, driven by the population dynamics model. The establishment chance (P_{est}), was equal to 1% (Equation 2), representative for a slow colonizer like *Spartina anglica* (Schwarz et al., 2018). The intrinsic growth rate of the vegetation (r) was equal to 1 per vegetation time step, which is in this study equal to a single hydrodynamic day and 100 morphodynamic days due to the use of an acceleration factor. The maximum stem density (K) was 1200 stems m^{-2} (van Hulzen et al., 2007) (Equation 4).

First the vegetation establishment, $(\partial n_b/\partial t)_{est}$ was calculated (Equation 2). The subsequent growth and decay (Equations 3–6) in the next vegetation timestep was solved using an ordinary differential equation solver, iterating toward the solution (c.f. Soetaert et al., 2010).

2.4. Model Scenarios

Four extensive scenarios were simulated with different significant wave heights (H_s), resulting in a focused, but limited set of experiments. Marshes only affected by tidal flow were simulated without waves (significant wave height (H_s) of 0.00 m), whereas the influence of both waves and tidal flow were assessed for waves with a height (H_s) of 0.05, 0.10 and 0.15 m. The wave period (Tm_{01}) at the boundary was 1.79, 2.53 and 3.10 s respectively, based on a constant wave steepness of 0.01. A suspended sediment concentration of 10 mg/L was imposed at the boundary for all four scenarios. The suspended sediment concentration was varied for the scenario with a significant wave height of 0.10 m, since this wave height is closest to values occurring in the field (Callaghan et al., 2010; Willemsen et al., 2018). The SSC imposed at the boundary were continuous and equal to 10, 25 and 50 mg/L. The scenario runs covered a period of 50 years. The first 10 years of the 50 years development were used to start-up the full model. This start-up time for the hydrodynamic, morphodynamic and vegetation module was used to initiate feedback between modules and prevent possible excessive dynamics being included in the analysis. The computational time of a single run was limited to approximately 5 days (2 cores @ 3.50 GHz; 32 GB memory).

3. Results

3.1. Salt Marsh Development and Marsh-Edge Patterns After 50 Years Under Different Wave Conditions

After 50 years of development in the model, of which 10 years start-up time, vegetation at the salt marsh edge revealed distinct features typically occurring at salt marshes in the field (Figures 1 and 3). The form and presence of those features depended on the incoming wave forcing at the seaward boundary. In the absence of wave forcing (H_s of 0.00 m) resulted in the formation of creeks landward from the vegetation edge (Figures 3a–3c). The creeks extended landward with multiple branches over a cross-shore width of 200 m. The large creeks showed an alongshore spacing of approximately 100 m. Moreover, vegetation patches with a diameter ranging from approximately 5 m (the size of a single computational cell) to 50 m were found seaward from the salt marsh edge (Figures 3a–3c).

In year 50, a sawtooth pattern was observed after salt marsh development with a wave forcing of 0.05 m (Figures 3d–3f), approximately at the same cross-shore location as the marsh edge developed without waves. Four to five coves formed over an alongshore distance of 1,000 m. An area with vegetation patches formed seaward from the marsh edge. Nevertheless, the cross-shore width of the area with patches was smaller than the area with patches resulting from the run without waves. The smaller area of patches might be explained by the steepness of

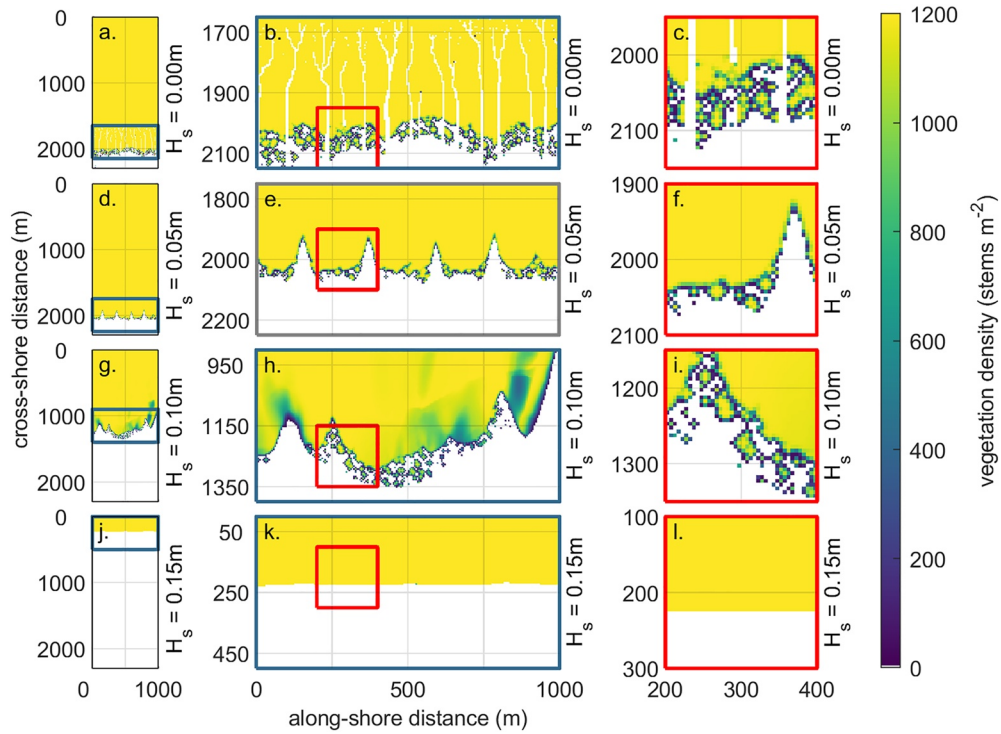

Figure 3. The vegetation density at the salt marsh in year 50, with a significant wave height of 0.00, 0.05, 0.10 and 0.15 m (from top to bottom). The full model domain is visualized in the left panels with the blue box indicating a zoom window around the vegetation edge. The zoom of the vegetation edge is highlighted in the second column. A zoom (red box) indicating the different features at the salt marsh edge is highlighted in the right panels. Note that the cross-shore location of the marsh edge in year 50 is different, depending on the wave forcing (see left panels and *y*-axis of the second and third row).

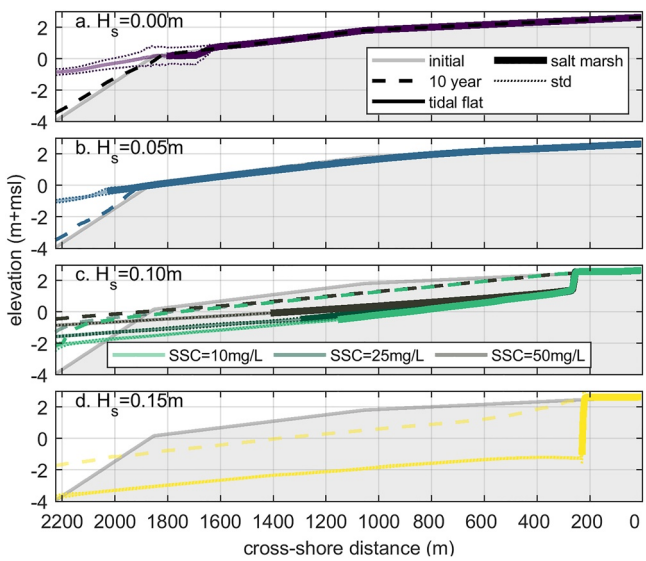

Figure 4. Alongshore averaged profiles initially, after 10-year spin-up and after 50 years under different wave forcing and sediment availability. The top panels highlight the results of the development of the bare tidal flat and vegetated salt marsh for a wave height of (a) 0.00 m (no wave), (b) 0.05 m, (c) 0.10 m with different suspended sediment concentrations and (d) 0.15 m.

the profile just seaward of the marsh edge, which is largest for the scenario with waves of 0.05 m (Figure 4), preventing extensive vegetation patches to develop.

The development of the salt marsh edge under a wave forcing of 0.10 m (Figures 3g–3i) showed similarities with the development of the marsh edge under a significant wave height of 0.05 m (i.e., Figures 3d–3f). A sawtooth pattern developed with vegetation patches appearing seaward from the marsh edge. However, the alongshore variability of both the patterns and the patches was larger. Moreover, a gradient of vegetation density formed in the alongshore direction (Figures 3g–3i).

The marsh edge showed no pattern at all in the model scenario with the largest wave forcing (H_s is 0.15 m; Figures 3j–3l). The straight marsh edge was formed as no new vegetation was able to establish in front of the existing marsh edge due to the larger waves, as visible from the abrupt transition from 1200 to 0 stems m^{-2} at the edge.

Creeks were absent in the model scenarios with waves, except when sediment supply increased (Figure 5; H_s = 0.10 m). This might be explained by sediment transport toward the vegetated salt marsh, preventing further development of creeks after initiation. Either by filling in initiated creeks with sediment or obstructing the locations where creek outlets appear.

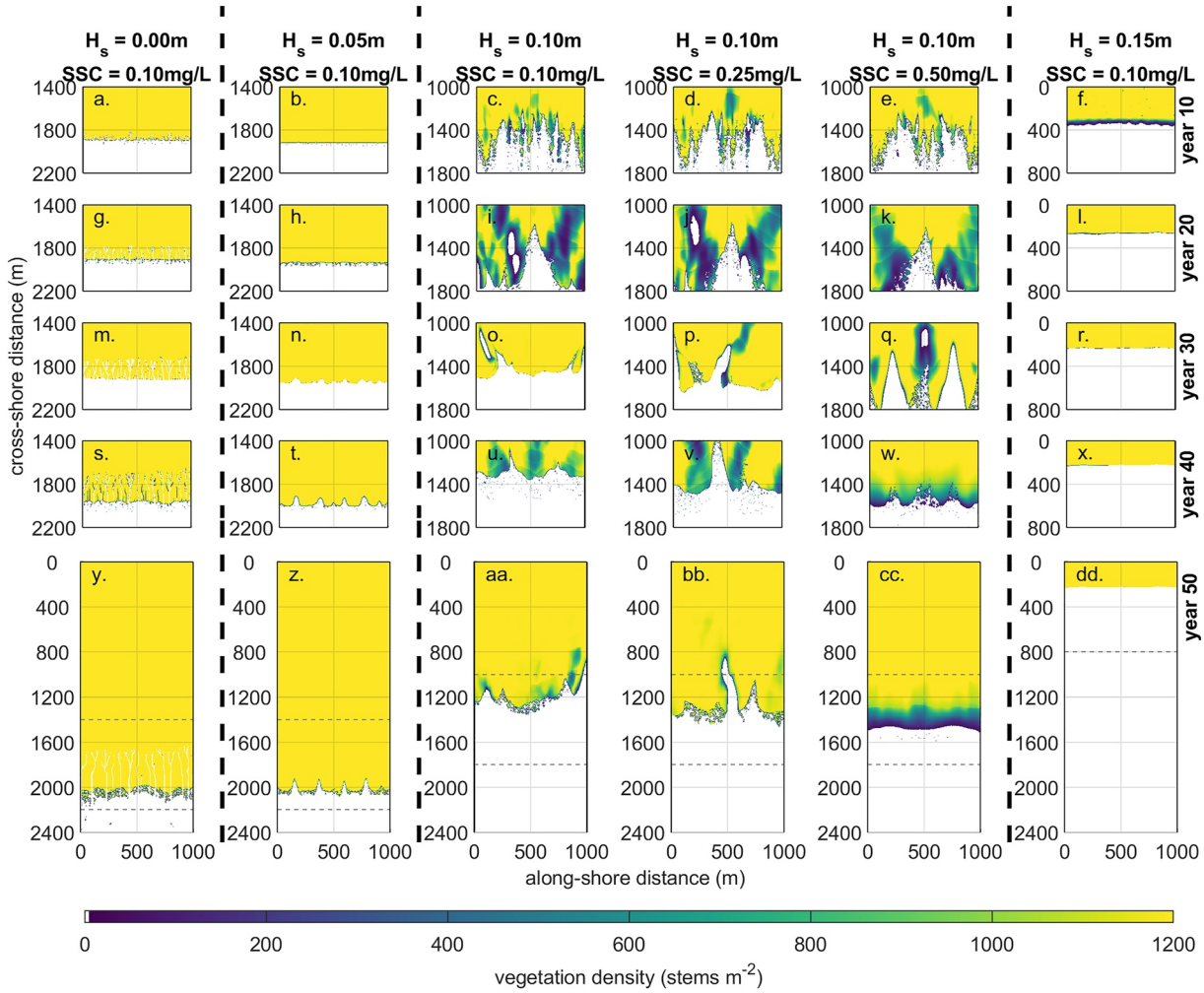

Figure 5. The development of the vegetation density (colormap) at the salt marsh edge per 10 years (from top to bottom). The resulting vegetation density in year 50 is presented for the full domain (bottom row). The area around that is presented in the first four rows of panels is indicated in the full domain (bottom row) with a dashed box. The different scenarios runs are presented from left to right.

3.2. Cross-Shore Profile Characteristics and Variability at the Parsh Edge

The development of the cross-shore profile was highly affected by the wave forcing and SSC (Figure 4). The alongshore averaged profile in year 50 remained rather similar to the initial profile with no wave and low wave forcing (0.00 and 0.05 m). With increasing wave forcing at the boundary (0.10 and 0.15 m), a cliff formed at the landward side of the domain, approximately 200 m from the landward boundary. Waves of $H_s = 0.10$ m, resulted in a cliff with a height of approximately 1.00 m, whereas wave forcing of 0.15 m resulted in a cliff with a height of 4.00 m (Figure 4). The wave height determines the general height of the profile, whereas the suspended sediment concentration determines the steepness of the profile (Figure 4). The alongshore variability of the profile in year 50 decreased with increasing wave heights (Figure 4; standard deviation). Smaller wave heights allowed patterns with large alongshore variability to develop (e.g., creek formation inside and outside the vegetated area and development of vegetation patches; Figures 3 and 5), resulting in larger alongshore variability of the bed elevation (Figure 6). Over time, the development of the vegetated salt marsh after initial establishment largely depended on the wave forcing. Without waves and with small waves (0.00 and 0.05 m), the salt marsh extended seaward, while the salt marsh retreated landward with larger wave forcing (0.10 and 0.15 m; Figure 5). However, with larger SSC, vegetation at the marsh was able to switch from a retreating to an extending behavior (H_s is 0.10 m; Figure 5). The salt marsh edge in year 50 was found at higher elevations with decreasing stress from waves and sediment availability (Figure 4), hence indicating the direction of development: a too low elevated salt marsh edge due to

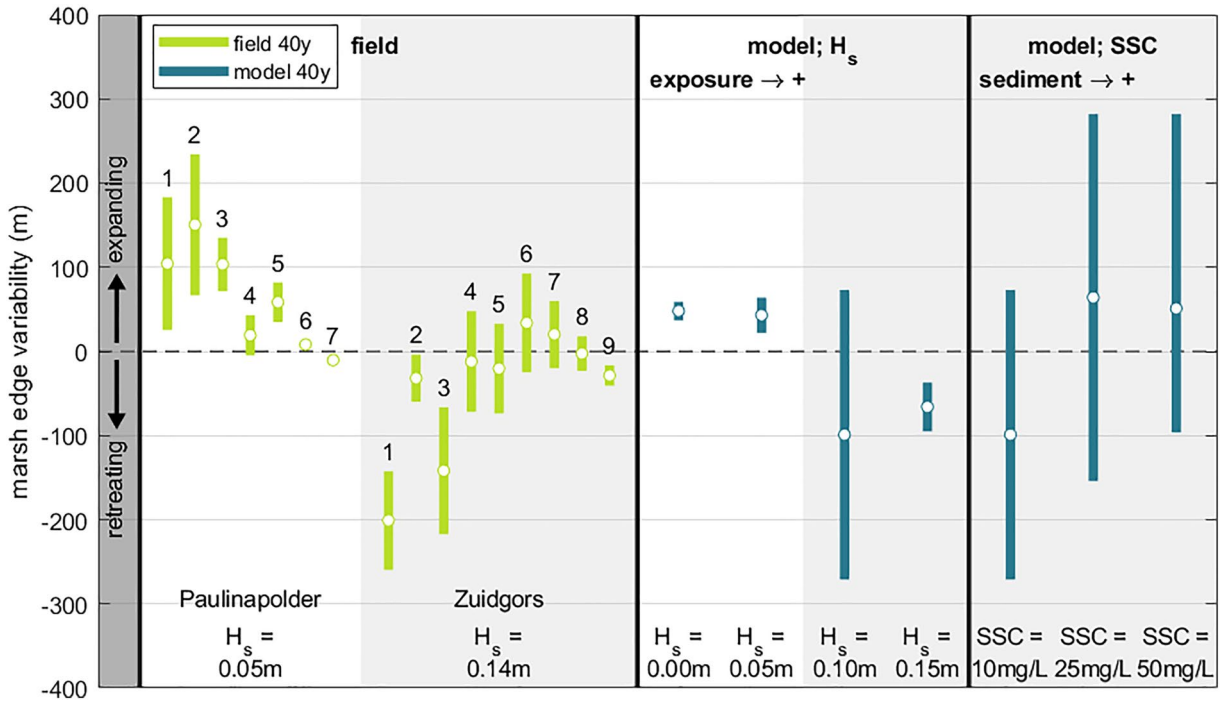

Figure 6. Variability of the marsh edge, that is, mean location of the marsh edge (white marker) and standard deviation (bar); from field data (left part of the figure) in the period 1975–2015 and from the model over a period of 40 years (year 10 to year 50) (right part of the figure). Numbers above the bars correspond to the transects shown in Figure 1. The results are sorted with an increasing wave exposure (from left to right); the model results with a default suspended sediment concentration of 10 mg/L, and increasing sediment availability (right part; from left to right). The marsh edge retreats if the variability is negative, whereas the marsh edge expands if the variability is positive.

continuously occurring physical stress retreats, whereas low levels of physical stress result in a higher salt marsh edge that can even expand. This balance suggests the importance of the response time of vegetation to physical stresses.

The final location of vegetation presence at the salt marsh edge was quickly reached for the lower wave heights (0.00 and 0.05 m), a slight seaward extension of tens of meters only was observed over the last four decades (Figure 5). Nevertheless, differences were observed in the development of vegetated salt marshes with larger wave heights (0.10 and 0.15 m): the occurrence of a cliff in the bathymetry largely affected vegetation growth. Vegetation was still able to establish in front of the cliff with $H_s = 0.10$ m over a cross-shore width of over 1000 m, although the variability of the vegetation density in this area was rather high due to the wave forcing (200–1200 stems m^{-2}). Vegetation was not able to establish in front of the cliff with largest wave height (H_s is 0.15 m; Figure 5), resulting in an abrupt transition from a vegetation density of 1200 to a density of 0 stems m^{-2}. The latter resulted in a rather small decadal variability of the cross-shore location of the marsh edge (Figure 6). This deviates from the increasing variability of the location of the marsh edge with increasing wave heights between wave heights (H_s) of 0.00 and 0.10 m.

3.3. Comparing Modeled Marsh Edge Characteristics to Field Observations

To test the schematic model predictions, the variability of the marsh edge in the field was quantified using field data from the salt marshes Zuidgors and Paulinapolder in the Westerschelde estuary (Figure 1). Generally, over a 40 year period (1975–2015), the marsh edge at Zuidgors (exposed to the prevailing wind direction) retreated, whereas the marsh edge at Paulinapolder (sheltered from the prevailing wind direction) expanded (Figure 6). This can be explained by the hydrodynamic energy occurring in both systems. Generally high hydrodynamic energy results in increasing bed level dynamics, lower bed elevations and longer inundation periods; an environment in which vegetation is not able to establish. On the contrary, low hydrodynamic energy leads to less bed level dynamics and inundation periods remain rather small, giving vegetation the opportunity to establish (Bouma

et al., 2016; Willemsen et al., 2018). The mean wave height observed seaward from the marsh edge at the tidal flat, specifically during calm conditions was 0.14 m at Zuidgors (standard deviation of 0.06 m), versus 0.05 m at Paulinapolder (standard deviation of 0.03 m) (Callaghan et al., 2010).

An expanding marsh edge was observed (Figure 6) for the model scenarios both without wave forcing and with rather small continuous wave forcing (0.05 m). The modeled marsh edge expanded seaward over 50 m on average over a period of 40 years, which resembles the average variability of the marsh edge at Paulinapolder (Figure 6). However, the modeled standard deviation of the marsh edge variability is lower, but in the same order of magnitude (tens of meters), most probably due to a more variable wave climate in the field.

A retreating marsh edge was observed for the model scenarios with larger wave forcing (0.10 and 0.15 m), although with increasing sediment availability the marsh was also able to expand. This is supported by the field observations at the Zuidgors marsh, where transects both were expanding and retreating at a single marsh. The simulated marsh edge retreated landward by 120 m on average over a period of 40 years (0.10 and 0.15 m), but was also able to expand over a length of approximately 60 m with larger SSC, corresponding to the average variability of the marsh edge at the exposed marsh Zuidgors (Figure 6). The standard deviation of the marsh edge location for the model run with $H_s = 0.10$ m was larger than observed in the field with similar wave heights (Zuidgors), mainly caused by the possibility for vegetation to establish seaward from the developed cliff. Conversely, vegetation was not able to establish seaward from the cliff with H_s equal to 0.15 m, hence resulting in a lower standard deviation (Figure 6). Vegetation patches were observed in the model runs with no waves and smaller wave forcing (0.00, 0.05 and 0.10 m). Vegetation patches appearing in year 50 were similar in size (5–50 m) as the patches observed in the field (Figure 1e and 1f), although the amount of pioneer vegetation growing in patches generally decreases with larger wave heights in the model, which is observed in the field as well.

3.4. Biophysical Response of Marshes to Waves: Marsh Width, Height and Vegetation Patterns at the Marsh Edge

The salt marsh responded differently to different wave forcing. Different responses were observed for an increasing wave height, with a suspended sediment concentration of 10 mg/L: (a) the cross-shore marsh width and marsh platform height was largest in the absence of waves (Figure 7; panel a, b, c); (b) the marsh width and height remained rather similar, whereas the alongshore variability decreased with small waves ($H_s = 0.05$ m). Alongshore periodic vegetation patterns appeared at the marsh edge (Figure 5; $H_s = 0.05$ m); (c) Both the marsh width and height decreased with medium waves, since vegetation was not able to establish at a lower elevation ($H_s = 0.10$ m), and the alongshore variability of both largely increased (Figure 7; panel a, b, c). The cross-shore variability of vegetation density was observed (Figure 5; $H_s = 0.10$ m); and (d) the average marsh width and height further decreased with large waves ($H_s = 0.15$ m). Moreover, the variability of the marsh width and height decreased to almost zero (Figure 7; panel a, c), at the same time a lack of variability in vegetation density was observed (Figure 5; $H_s = 0.15$ m), since vegetation was almost not able to establish at lower heights (Figure 7; panel b).

The modeled cross-shore width of the salt marsh was affected by wave height (H_s). The mean width was approximately 2000 m for low wave heights (Hs is 0.00 and 0.05 m). Once the wave height increased to $H_s = 0.10$ m and larger, initiation of cliff formation was observed (Figure 4) and the width of the salt marsh decreased to 1300 m ($H_s = 0.10$ m) and 220 m ($H_s = 0.15$ m). The salt marsh width was affected by cliff formation, with the appearance of cliffs depending on the wave forcing (Figure 7; panel a).

The mean height of the vegetated salt marsh platform changed with the incoming wave height as well (Figure 7; panel b). The height of the platform decreased with increasing wave heights. Although cliff formation was initiated when the wave height exceeded 0.10 m, a clear threshold affecting the height of the salt marsh platform was not observed for wave heights between $H_s = 0.00$ m and $H_s = 0.10$ m. The average height of the salt marsh platform decreased from 1.55 m + MSL to 1.49 m + MSL to 1.18 m + MSL. Once the wave height increased ($H_s = 0.15$ m), the platform height suddenly increased (2.60 m + MSL).

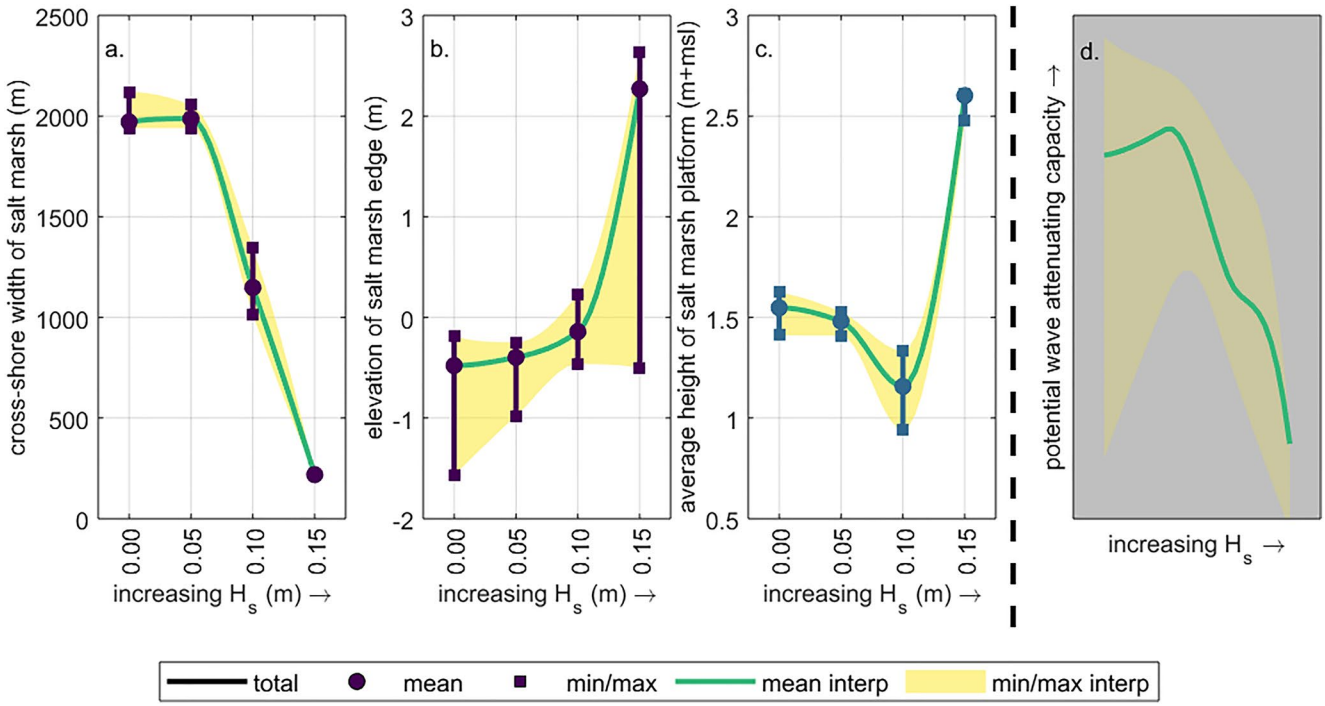

Figure 7. (a) Cross-shore width of the vegetated salt marsh, the height of the salt marsh edge (b) and the height of the salt marsh platform (c) for a suspended sediment concentration of 10 mg/L, averaged over the last 10 years of the model run. A qualitative impression of the potential wave attenuating capacity, as a result of the salt marsh extent, is outlined in panel d. and discussed in Section 4.2.

4. Discussion

Salt marshes are neither homogeneous, nor static (Reed et al., 2018). An understanding of the long-term marsh width dynamics is required to predict their dynamic capacity to attenuate waves and implement marshes in hybrid flood defenses (Bouma et al., 2014, 2016; Willemsen et al., 2020). Like previous studies into salt marsh extent (e.g., Leonardi et al., 2016; Marani et al., 2011; McLoughlin et al., 2015), this current study showed that vegetation dynamics around the salt marsh edge depend on wave forcing and sediment supply. Seaward salt marsh expansion required low or moderate wave forcing or high sediment supply. Alternatively, when the wave forcing was high and sediment supply limited the salt marsh retreated landward. With increasing sediment availability the salt marsh forced with higher waves was able to switch from a retreating extent toward an expanding extent.

4.1. Biogeomorphological Modeling of the Salt Marsh Width

Previous numerical modeling studies identified processes driving salt marsh development, for example, on a two dimensional (depth-averaged) and three dimensional landscape scale (Best et al., 2018; Temmerman et al., 2007). Similar model studies addressed salt marsh development on a timescale of centuries aiming to assess salt marsh development and/or loss due to SLR and changes in sediment availability (D'Alpaos & Marani, 2016; Kirwan & Murray, 2007; Kirwan et al., 2010; Mariotti & Canestrelli, 2017). Mariotti and Canestrelli (2017) highlighted that, instead of platform drowning, retreat of the salt marsh edge will likely cause marsh loss on a timescale of centuries. Furthermore, simplified models indicated that the salt marsh edge may retreat due to wave-induced cliff erosion (e.g., Tambroni & Seminara, 2012), thereby enabling marsh loss. Process-based models that focused on the marsh edge showed a similar relation between wind waves and marsh retreat (Mariotti & Fagherazzi, 2013; Marani et al., 2011). However, wind waves have not always been included in models describing salt marsh development (Belliard et al., 2015; Temmerman et al., 2005, 2007). The current study builds upon and extends these previous studies, by using a process-based vegetation model, resulting in a more realistic progradation regime and vegetation decay.

Salt marsh width is variable over time, and the salt marsh edge can retreat landward or expands seaward by several meters a year (Allen, 2000; Cox et al., 2003; Francalanci et al., 2013; Wang et al., 2017). More specifically in the Westerschelde estuary, a general landward retreat of the salt marsh edge is observed at Zuidgors and Zimmermanpolder at its northern shores from 1982 till 2004, whereas a general expanding trend of the salt marsh edge is observed at Paulinapolder and other salt marshes at the southern shores over the same period (Van der Wal et al., 2008). Differences between sites may be related to their relative wind exposure. The salt marshes at the northern shores of the Westerschelde estuary are classified as exposed to the prevailing south-westerly winds (e.g., Zuidgors), whereas the salt marshes at the southern shores (e.g., Paulina) are more sheltered from these winds (Callaghan et al., 2010). Whilst the daily variability of wave heights was not considered in the present study (i.e., we used a homogeneous wave height to clearly distinguish between processes that affect the salt marsh width), the modelled variability of the marsh edge position corresponded well with field observations (Figure 6). Despite the similarity of the modeled and observed marsh width variability in the present study, the range of marsh width for a medium wave height ($H_s = 0.10$ m) and the height of the cliff for a large wave height ($H_s = 0.15$ m), did deviate from field observations. Previous studies quantified a relation between wave power density and cliff retreat (e.g., Leonardi et al., 2016; Marani et al., 2011; Schwimmer, 2001; Stecca et al., 2017). The relation between wave power density and marsh edge retreat rate in the current study was rather weak ($H_s = 0.10$ m; $R^2 = 0.15$). With a wave height of 0.10 m vegetation was able to grow seaward of the vegetation edge, which resulted in a horizontal offset between the cliff and actual marsh edge. Pioneer vegetation that colonized the tidal flat in front of the former salt marsh, suggested the presence of a mechanism that can drive a retreating into an expanding salt marsh (c.f. Singh Chauhan, 2009). The relation between wave power density and marsh edge retreat was slightly better for a wave height of 0.15 m ($R^2 = 0.23$), where the marsh edge was at the same location as the cliff. Building on previous studies (Leonardi & Fagherazzi, 2014; Mariotti, 2020; Mariotti & Canestrelli, 2017), in future studies the use of a sophisticated cliff erosion model combined with a process-based vegetation growth model is recommended and will result in improved predictions of marsh edge retreat due to cliff erosion. If a cliff erosion model had been implemented in the current study, the predicted cliff height would likely have been smaller due to faster retreat and deposition of material originating from the cliff in front of the cliff. Consequently, integrating a cliff erosion model would have resulted in a better representation of field observations.

The horizontal marsh width variability would have been smaller if the wave forcing would have been more variable, that is, hourly changing wave heights. This would have led to a smaller range of marsh width variability for model simulations with medium waves and less extreme cliff heights for model simulations with large waves. Short events with extreme waves, which were not included in the model simulations, may have resulted in more disturbances of the bed, thereby decreasing the frequency and duration of calm periods in which vegetation could establish (Hu et al., 2015). Hydrodynamic exposure and bed level change will increase during large wave events and, thereby increasing vegetation mortality (Temmerman et al., 2007) and landward retreat of the marsh edge (Bouma et al., 2016; Willemsen et al., 2018). Conversely, during periods with rather small waves in a variable wave climate the establishment of vegetation will not be disturbed and therefore vegetation development is enhanced (Bouma et al., 2016), resulting in a seaward expanding salt marsh.

In the present study a MorFac of 100 was applied to decrease computational time and accelerating morphological development. A sensitivity analysis was conducted to assess the influence of the MorFac on the vegetation development and the dynamics of the salt marsh edge. The MorFac was multiplied by a factor 2 (MorFac = 200) and divided by a factor 2 (MorFac = 50). Furthermore, simulations were executed with (case 1) a fixed factor for the vegetation update and (case 2) an adapted factor for the vegetation update, related to the adapted MorFac. With the higher MorFac and a fixed factor for the vegetation update (case 1), the dynamics of the salt marsh edge were found to increase and the rate of retreat increased. The observed increasing rate of retreat can be explained by larger erosion rates that increasingly exposed the establishing vegetation. Nevertheless, differences in simulated retreat rates remained small between a MorFac of 50 and 100 (maximum of tens of meters over a domain of 2,500 m). When a corrected factor for vegetation development updates was applied with changing the MorFac (case 2), the location of the salt marsh edge remained similar over time for a MorFac of 50 and 100, but it changed substantially for a MorFac of 200. The sensitivity analysis showed that the applied vegetation model is robust when using a MorFac of 100 and lower, but a MorFac of 200 with the current model set-up showed strongly deviating results. Following this sensitivity analysis, the use of a MorFac of 100 in the current study is justified.

More processes were simplified in this model exploration. For example, critical bed shear stresses for erosion were kept constant, even though it is known that the bed becomes stronger with the increasing duration of vegetation presence in a certain area (Wang et al., 2017). Furthermore, the default suspended sediment concentration imposed at the boundary of the model was in the lower range of the sediment concentrations occurring in the Westerschelde estuary. In general, salt marsh width and platform height are smaller with low SSC and increase with increasing SSC (Mariotti & Fagherazzi, 2010; Temmerman et al., 2004). This study showed that, with feedback between hydrodynamics, morphodynamics and vegetation growth, increasing sediment concentrations resulted in a higher marsh platform due to enhanced sedimentation on the platform compared to previous studies (c.f. Mariotti & Fagherazzi, 2010; Temmerman et al., 2004) The lower wave exposure of the elevated marshes will enhance vegetation growth, enabling the marsh to maintain its position over a longer period. However, a higher marsh platform might be more prone to lateral erosion due to a larger vertical offset between bare tidal flat and salt marsh. This increasing instability could be better assessed by including a process-based cliff-erosion model.

The tide, consisting of S2 and M2 tidal constituents, was explicitly chosen to be equal in all scenarios. Therefore, the influence of tides and tidal range on the dynamics of the salt marsh edge was not assessed. Generally, the seaward extent of the salt marsh is limited by mean high water (Adam, 2002). Balke et al. (2016) showed that the marsh edge is able to extend further seaward with an increasing tidal range. The stability of the vegetated platform also improves with an increasing tidal range, as the growth range of vegetation increases with tidal range (Kirwan & Guntenspergen, 2010; D'Alpaos et al., 2011). This might be attributed to increasing dispersion of hydrodynamic energy with an increasing tidal range as wave energy will be distributed over a wider area of the salt marsh, instead of being focused at the salt marsh edge. Accordingly, it can be assumed that waves have a larger influence on the salt marsh width in microtidal estuaries. The computational domains of the flow and wave model that were used in this study prevented for boundary effects from occurring, as evidenced by the results (e.g., Figure 5). Morphology and vegetation dynamics were consistent throughout the flow domain. The resolution of the grid (grid cell size) was sufficiently high to prevent for numerical effects on the hydrodynamics (Bomers et al., 2019). However, the grid cell size may have hampered smaller scale dynamics, for example, small-scale creek development, although this was not the focus of the current study.

Next steps in the development and assessment of the model should be focusing on the implementation of a variable wave climate and/or sediment availability to extend on the homogeneous wave forcing and sediment availability. These improvements will allow to use the vegetation model to its full capacity, as variable wave forcing and sediment availability inherently lead to increasingly variable stresses, enabling greater dynamics in the establishment of vegetation. Furthermore, different vegetation species with different traits could be incorporated. Currently, a slow colonizer with clonal growth was simulated (*Spartina anglica*). However, fast colonizers without the ability of clonal growth (e.g., *Salicornia europaea*) can also be simulated with the current model (c.f. Schwarz et al., 2018). The latter species grows faster initially, but its biomass declines over the winter period, and hence explicit seasonality is required to model this species. For inclusion of different species and to improve single-species simulations, belowground feedback between morphology and vegetation, that is, spatio-temporal differences in substrate strength (Chirol et al., 2021), is required. This can be simulated by implementing a spatio-temporal varying critical bed shear stresses. Eventually, such model adaptations for vegetation species will lead to different predictions of vegetation patterns and landscape morphology, for example, less patchy patterns with *Salicornia europaea* (slow colonizers without clonal growth), right from the early stages of initial establishment.

4.2. Implications for Nature-Based Flood Defenses

An important ecosystem service of salt marshes is their wave attenuating capacity, which increases coastal safety locally (Temmerman et al., 2013). NBFD incorporate the protective functionality of ecosystems. The reduction of the significant wave height (i.e., wave attenuating capacity) of a vegetated foreshore can be explained by the width of the vegetated foreshore and the reduced water depth over such accreted vegetated foreshores (e.g., Möller & Spencer, 2002; Vuik et al., 2016; Willemsen et al., 2020). The current model results indicated the development of wider vegetated foreshores at places with less wave forcing and increasing sediment availability. Moreover, the model results highlighted a decreasing height of the marsh platform with larger wave forcing, until the cliff exceeded a certain height and vegetation was not able to grow seaward from the cliff. When the relations of the imposed wave exposure and modeled marsh dimensions are combined, a general non-linear trend

was observed: the development of salt marshes under larger wave heights might lead to a smaller potential wave attenuating capacity (Figure 7; qualitative impression in panel d.). Still, the wave attenuating capacity related to a simulated average wave height of 0.10 m, which typically occurs at salt marshes in the Westerschelde, is relatively large (Willemsen et al., 2018).

This study emphasized once more that the widest salt marshes occur in the lowest-energy environments, which are sheltered from incoming high waves. Although salt marshes expand when the sediment availability increases, it would appear that the extent of any such increase is limited, most probably due to an increasing offset between the bare tidal flat and vegetated salt marsh with an expanding marsh. The cross-shore width of the salt marsh decreased with increasing wave heights. In the low-energy environments where salt marshes thrive, they can contribute to the wave attenuation of extreme storm events, provided that their cross-shore width is sufficiently large (Vuik et al., 2016). Not surprisingly, even though wide salt marshes are very effective at wave attenuation, they generally occur only where waves are small. However, the area of application might largely increase by enhancing marsh growth with engineering measures and using salt marshes as part of a NBFD (e.g., Baptist et al., 2021; Vuik et al., 2019).

Artificial structures like brushwood dams can assist in enhancing vegetation establishment and growth. Lower wave heights enable salt marsh vegetation to establish (Poppema et al., 2019), by decreasing bed level dynamics (Bouma et al., 2016; Cao et al., 2018) and seedling mortality (Cao et al., 2019). This is also observed in this study. Lower wave heights support vegetation establishment at a lower elevation (Figure 7; panel b). Additionally, a decreasing inundation period and frequency leads to better opportunities for vegetation growth (Balke et al., 2016); Structures will promote settling of suspended sediments, which increases the bed level (Siemes et al., 2020); The wave height at the landward side of artificial structures is observed to be generally lower, and frequently occurring small waves are generally absent. Hence, artificial structures will lead to a larger marsh width due to the absence of small continuous waves. The enhanced larger salt marsh width will result in a larger contribution to wave attenuation (Willemsen et al., 2020).

There is a paradox both in the model result predicting continuous retreat of the vegetated salt marsh edge and in observations confirming such retreat over decadal timescales. Before a salt marsh can expand, the conditions must be favorable for vegetation to develop and expand seaward. Some elements in the landscape should, at least during certain periods of time, permit the salt marsh to develop before it enters into a phase of retreat. Tidal flats in front of salt marshes are candidate landscape elements for that. Tidal flats can effectively dissipate wave energy under daily conditions (Callaghan et al., 2010), which improves the conditions for salt marsh development at the landward side. Seaward expansion of tidal flats were observed to be a consequence of spatial shifts in tidal channels, or changes in sediment availability. Increasing the accommodation space for intertidal systems or stimulating growth of tidal flats with engineering measures, might enhance seaward expansion of salt marshes (Bouma et al., 2016; Callaghan et al., 2010). Stimulating sedimentation at tidal flats with, for example, sediment disposals and nourishments has resulted in a switch from an erosive phase to an accreting phase (de Ve et al., 2020), as is also observed for salt marshes in the current study. This is also confirmed by the long-term analyses by Ladd et al. (2019) who showed that marsh width over the last 150 years in 25 estuaries and embayments spread over the UK, critically depended on SSC. An accreting tidal flat might lead to a decreasing daily wave height at the marsh. Lower wave heights at the marsh edge have resulted in expanding salt marshes, based on the results of the current study and experimental studies on marsh establishment (Cao et al., 2019; Hu et al., 2015; Zhu, van Belzen, et al., 2020). Furthermore, vegetation patterns, such as patches and gradients in density at the marsh edge, showed the possibility for establishment of pioneer vegetation, thereby emphasizing the resilience of the salt marsh at lower wave heights. An increasing salt marsh width leads to a larger wave attenuating capacity (Vuik et al., 2016; Willemsen et al., 2020), hence enabling the use of saltmarshes in NBFDs.

5. Conclusions

A biogeomorphological model with a process-based vegetation growth module was presented to assess the dynamic cross-shore salt marsh width. Salt marsh development was modeled over a period of 50 years schematically forced with waves and differences in sediment availability. The development was assessed to answer the key question: How does the biophysical development, cross-shore width and yearly variability of a vegetated salt marsh depend on the magnitude of hydrodynamic forcing and sediment availability over a decadal time scale?

Under average mild weather conditions, the salt marsh width was intrinsically vulnerable to erosion. In year 50, with increasing physical stress, the salt marsh edge was found at lower elevations, indicating an unhealthy system with a retreating marsh edge due to vegetation mortality, whereas decreasing physical stresses result in a higher salt marsh edge enabling expansion after 50 years of development. This balance suggests the importance of the response time of vegetation to physical stress. The variability of the salt marsh edge increases up until a point vegetation is not able to establish in front of the marsh edge. The vegetation density gradient and patterns around the marsh edge increase up till the same point. Furthermore, small changes in the magnitude of sediment availability, result in rather large variability in marsh width, enabling even to transform from a retreating marsh to expansion. The results suggest a resilient marsh edge where re-establishment is possible for locations with rather small mild wave conditions, but with little increase of wave height only, vegetation decays and the marsh almost fully retreats. So while conventional gray coastal infrastructure can be applied generically, salt marshes in NBFDs are more location-specific due to spatially variable conditions. These model studies inspire management measures and artificial structures for enhancing the development of tidal flat–salt marsh systems.

Appendix A: Hydrodynamic and Morphodynamic Model Equations

Hydrodynamic and morphodynamic processes in the current study are solved using the numerical Delft3D-FM model (Deltares, 2019a, 2019b; 2019c). Both hydrodynamics and morphodynamics interact with the vegetation module via BMI (Hutton et al., 2020), enabling simulations of ecosystem development in the coastal zone.

A1.1 Flow Module

Delft3D-FM solves the Navier-Stokes equations for an incompressible fluid, under the shallow water assumptions (i.e., hydrostatic pressure) and Boussinesq approximation (The effect of variable density is only taken into account in the pressure term) (Deltares, 2019a):

$$\frac{\partial u}{\partial t} + u\frac{\partial u}{\partial x} + v\frac{\partial u}{\partial y} + w\frac{\partial u}{\partial z} = -\frac{1}{\rho_0}\frac{\partial p}{\partial x} + \nu\Delta u - f_x \tag{A1}$$

$$\frac{\partial v}{\partial t} + u\frac{\partial v}{\partial x} + v\frac{\partial v}{\partial y} + w\frac{\partial v}{\partial z} = -\frac{1}{\rho_0}\frac{\partial p}{\partial y} + \nu\Delta v - f_y \tag{A2}$$

$$\frac{\partial w}{\partial t} + u\frac{\partial w}{\partial x} + v\frac{\partial w}{\partial y} + w\frac{\partial w}{\partial z} = -\frac{1}{\rho_0}\frac{\partial p}{\partial z} + \nu\Delta w - f_z - \frac{\rho}{\rho_0}g \tag{A3}$$

where u, v and w present the velocity components in x-, y- and z-direction respectively. ρ and ρ_0 the density and initial density respectively, p the pressure, ν the kinematic viscosity, f_x, f_y and f_z represent the components of the Coriolis force and g is the gravitational force.

The continuity equation can be derived assuming mass conservation:

$$\frac{\partial u}{\partial x} + \frac{\partial v}{\partial y} + \frac{\partial w}{\partial z} = 0 \tag{A4}$$

The model setup in the current study uses a two dimensional (depth-averaged) approach, assuming that vertical accelerations are sufficiently small to be neglected, thereby reducing the rate of change in the vertical to the hydrostatic pressure distribution:

$$\frac{\partial p}{\partial z} = -\rho g \tag{A5}$$

By elaborating the viscous stresses in Equations A1 and A2 and substituting Equation A5:

$$\frac{\partial h}{\partial t} + \frac{\partial hu}{\partial x} + \frac{\partial hu}{\partial y} = 0 \tag{A6}$$

$$\frac{\partial u}{\partial t} + u\frac{\partial u}{\partial x} + v\frac{\partial u}{\partial y} + g\frac{\partial h}{\partial x} - fv + \frac{1}{\rho_0}\left(\frac{\partial \tau_{xx}}{\partial x} + \frac{\partial \tau_{xy}}{\partial y} + \frac{\partial \tau_{bx}}{h}\right) = 0 \tag{A7}$$

$$\frac{\partial v}{\partial t} + u\frac{\partial v}{\partial x} + v\frac{\partial v}{\partial y} + g\frac{\partial h}{\partial y} - fu + \frac{1}{\rho_0}\left(\frac{\partial \tau_{yx}}{\partial x} + \frac{\partial \tau_{yy}}{\partial y} + \frac{\partial \tau_{by}}{h}\right) = 0 \tag{A8}$$

where τ_b is the bed shear stress and h the water depth.

Vegetation effects on hydrodynamics are accounted for by implementing the roughness predictor by Baptist, et al. (2007). The resulting bed roughness (C) and the flow resistance of the vegetation (λ) are calculated using the following equation (Deltares, 2019a):

$$C = C_b + \frac{\sqrt{g}}{\kappa}\ln\left(\frac{h}{h_{\text{veg}}}\right)\sqrt{1 + \frac{C_D n_b h_{\text{veg}} C_b^2}{2g}} \tag{A9}$$

$$\lambda = C_D n_b \frac{h_{\text{veg}}}{h}\frac{C_b^2}{C^2} \tag{A10}$$

where C_b is the bed roughness of the bare bed, κ is the von Kármán constant, h_{veg} is the stem height, C_D the drag coefficient and n_b the stem density. These equations are valid both for emergent and submerged vegetation. So the effect of vegetation on hydrodynamics is parameterized in a bed roughness, consequently affecting bed shear stresses.

A1.2 Wave Module

The wave module is used to simulate the evolution of random, short-crested wind-generated waves. In the wave module, waves are described with the two dimensional wave action density spectrum, since in the presence of currents, action density is conserved (Deltares, 2019c). The evolution of the wave spectrum is described by the spectral action balance equation in Cartesian coordinates (Hasselmann, et al., 1973):

$$\frac{\partial}{\partial t}N + \frac{\partial}{\partial x}c_x N + \frac{\partial}{\partial y}c_y N + \frac{\partial}{\partial_\sigma}c_\sigma N + \frac{\partial}{\partial \theta}c_\theta N = \frac{S}{\sigma} \tag{A11}$$

The local rate of change of action density is represented by the first term, propagation of action in geographical space (with propagation velocities c_x and c_y in x- and y-direction) is represented by the second and third term respectively. Shifting of the relative frequency due to variations in depths and currents (with propagation velocity c_σ in σ-space) is represented by the fourth term and the fifth term represents dept-induced and current-induced refraction (with propagation velocity c_θ in θ-space). Expressions for these propagation speeds are taken from linear wave theory. The term at the right-hand side, where S (=(S (σ, θ)), is the source term in terms of energy density representing the effects of generation, dissipation and non-linear wave-wave interactions (Deltares, 2019c).

Wave dissipation by vegetation is included as a source term (Méndez & Losada, 2004; Suzuki et al., 2012) in the wave module:

$$S_{ds,\text{veg}} = -\sqrt{\frac{2}{\pi}}g^2 \tilde{C}_D b_{\text{veg}} n_b \left(\frac{\tilde{k}}{\tilde{\sigma}}\right)\frac{\sinh^3 \tilde{k}h_{\text{veg}} + 3\sinh \tilde{k}h_{\text{veg}}}{3k\cosh^3 \tilde{k}h}\sqrt{E_{\text{tot}}}E(\sigma,\theta) \tag{A12}$$

where $\tilde{C}_D$ is the drag coefficient, b_{veg} the stem diameter of vegetation, n_b the stem density of vegetation, $\tilde{k}$ the mean wave number, $\tilde{\sigma}$ the mean frequency, h_{veg} the vegetation height, E_{tot} the total energy and E (σ, θ) the energy over wave frequency and direction.

A1.3 Morphodynamic Module

In the model, cohesive sediments are assumed to be transported as suspended load, which is computed by the advection-diffusion equation:

$$\frac{\partial c}{\partial t} + \frac{\partial uc}{\partial x} + \frac{\partial vc}{\partial y} + \frac{\partial (w - w_s)c}{\partial z} - \frac{\partial}{\partial x}\left(\epsilon_{s,x}\frac{\partial c}{\partial x}\right) - \frac{\partial}{\partial y}\left(\epsilon_{s,y}\frac{\partial c}{\partial y}\right) - \frac{\partial}{\partial z}\left(\epsilon_{s,z}\frac{\partial c}{\partial z}\right) = 0 \tag{A13}$$

where c is the mass concentration of the sediment fraction, u, v and w are the flow velocity components in x, y and z direction, $\epsilon_{s,x}$, $\epsilon_{s,y}$ and $\epsilon_{s,z}$ are the eddy diffusivities of the sediment fraction and w_s is the settling velocity. In the current study with two dimensional (depth-averaged) settings, the fourth and seventh term reduce to zero.

Boundary conditions at the open boundary are prescribed by the user. Boundary conditions at the free surface and at the bed are set by the morphodynamic module. The vertical diffusive flux through the free surface is set to zero. So the water surface boundary condition is given by:

$$-\boldsymbol{w_s c} - \epsilon_{s,z}\frac{\partial \boldsymbol{c}}{\partial \boldsymbol{z}} = 0, \quad \boldsymbol{at \;\; z = \zeta \;\; (free \;\; surface)} \tag{A14}$$

The exchange of material between the bed and water column is modeled by calculating the sediment fluxes from the water column to the bed and vice versa. The fluxes are incorporated in the model as source and/or sink term, also to account for morphological updating. The boundary condition at the bed is given by:

$$-\boldsymbol{w_s c} - \epsilon_{s,z}\frac{\partial \boldsymbol{c}}{\partial \boldsymbol{z}} = \boldsymbol{D - E}, \quad \boldsymbol{at \;\; z = z_b \;\; (bed \;\; level)} \tag{A15}$$

where E is the erosion flux and D the deposition flux. For cohesive sediments, both fluxes are calculated with the Partheniades-Krone formulations (Partheniades, 1965):

$$\boldsymbol{E} = \begin{cases} M\left(\dfrac{\boldsymbol{\tau_{b,\max}}}{\boldsymbol{\tau_{\mathrm{cr},e}}} - 1\right), & \text{when } \boldsymbol{\tau_{b,\max} > \tau_{\mathrm{cr},e}} \\ 0, & \text{when } \boldsymbol{\tau_{b,\max} \le \tau_{\mathrm{cr},e}} \end{cases} \tag{A16}$$

$$\boldsymbol{D} = \begin{cases} \boldsymbol{w_s c}\left(1 - \dfrac{\boldsymbol{\tau_{b,\max}}}{\boldsymbol{\tau_{\mathrm{cr},d}}}\right), & \text{when } \boldsymbol{\tau_{b,\max} < \tau_{\mathrm{cr},d}} \\ 0, & \text{when } \boldsymbol{\tau_{b,\max} \ge \tau_{\mathrm{cr},d}} \end{cases} \tag{A17}$$

where M is the erosion parameter, $\tau_{b,\max}$ is the maximum bed shear stress due to currents and waves, $\tau_{\mathrm{cr},e}$ is the critical bed shear stress for erosion, w_s is the settling velocity, c the average sediment concentration and $\tau_{\mathrm{cr},d}$ the critical bed shear stress for deposition.

Data Availability Statement

Data and scripts in support of this manuscript are available via DOI: 10.4121/13203644.

Acknowledgments
This work is part of the research program BE SAFE, which is financed by the Netherlands Organization for Scientific Research (NWO) (grant 850.13.010). Additional financial support has been provided by Deltares, Boskalis, Van Oord, Rijkswaterstaat, World Wildlife Fund, and HZ University of Applied Science. Bas W. Borsje was supported by the Netherlands Organization for Scientific Research (NWO-STW-VENI; 4363). We would like to thank A. Mourits for his contribution to the technical development of the model and T. van Veelen and E. Horstman for their valuable comments. We are grateful for receiving the extensive comments of three reviewers.

References

Achete, F. M., van der Wegen, M., Roelvink, D., & Jaffe, B. (2016). Suspended sediment dynamics in a tidal channel network under peak river flow. *Ocean Dynamics*, *66*(5), 703–718. https://doi.org/10.1007/s10236-016-0944-0

Adam, P. (2002). Saltmarshes in a time of change. *Environmental Conservation*, *29*(1), 39–61. https://doi.org/10.1017/s0376892902000048

Allen, J. R. L. (2000). Morphodynamics of holocene salt marshes: A review sketch from the Atlantic and southern North sea coasts of Europe. *Quaternary Science Reviews*, *19*(12), 1155–1231. https://doi.org/10.1016/s0277-3791(99)00034-7

Balke, T., Stock, M., Jensen, K., Bouma, T. J., & Kleyer, M. (2016). A global analysis of the seaward salt marsh extent: The importance of tidal range. *Water Resources Research*, *52*(5), 3775–3786. https://doi.org/10.1002/2015wr018318

Balke, T., Webb, E. L., van den Elzen, E., Galli, D., Herman, P. M. J., & Bouma, T. J. (2013). Seedling establishment in a dynamic sedimentary environment: A conceptual framework using mangroves. *Journal of Applied Ecology*, *50*(3), 740–747. https://doi.org/10.1111/1365-2664.12067

Baptist, M. J. (2005). *Modelling floodplain biogeomorphology*. DUP Science.

Baptist, M. J., Babovic, V., Rodríguez Uthurburu, J., Keijzer, M., Uittenbogaard, R. E., Mynett, A., & Verwey, A. (2007). On inducing equations for vegetation resistance. *Journal of Hydraulic Research*, *45*(4), 435–450. https://doi.org/10.1080/00221686.2007.9521778

Baptist, M. J., Dankers, P., Cleveringa, J., Sittoni, L., Willemsen, P. W. J. M., van Puijenbroek, M. E. B., et al. (2021). Salt marsh construction as a nature-based solution in an estuarine social-ecological system. *Nature-Based Solutions*, *1*, 100005. https://doi.org/10.1016/j.nbsj.2021.100005

Belliard, J.-P., Toffolon, M., Carniello, L., & D'Alpaos, A. (2015). An ecogeomorphic model of tidal channel initiation and elaboration in progressive marsh accretional contexts. *Journal of Geophysical Research: Earth Surface*, *120*(6), 1040–1064. https://doi.org/10.1002/2015jf003445

Bendoni, M., Mel, R., Solari, L., Lanzoni, S., Francalanci, S., & Oumeraci, H. (2016). Insights into lateral marsh retreat mechanism through localized field measurements. *Water Resources Research*, *52*(2), 1446–1464. https://doi.org/10.1002/2015wr017966

Best, Ü. S. N., Van der Wegen, M., Dijkstra, J., Willemsen, P. W. J. M., Borsje, B. W., & Roelvink, D. J. A. (2018). Do salt marshes survive sea level rise? Modelling wave action, morphodynamics and vegetation dynamics. *Environmental Modelling & Software*, *109*, 152–166. https://doi.org/10.1016/j.envsoft.2018.08.004

Bomers, A., Schielen, R. M. J., & Hulscher, S. J. M. H. (2019). The influence of grid shape and grid size on hydraulic river modelling performance. *Environmental Fluid Mechanics*, *19*, 1273–1294

Booij, N., Ris, R. C., & Holthuijsen, L. H. (1999). A third-generation wave model for coastal regions: 1. Model description and validation. *Journal of Geophysical Research*, *104*(C4), 7649–7666. https://doi.org/10.1029/98jc02622

Borsje, B. W., van Wesenbeeck, B. K., Dekker, F., Paalvast, P., Bouma, T. J., van Katwijk, M. M., & de Vries, M. B. (2011). How ecological engineering can serve in coastal protection. *Ecological Engineering*, *37*(2), 113–122. https://doi.org/10.1016/j.ecoleng.2010.11.027

Bouma, T. J., De Vries, M. B., Low, E., Peralta, G., Tánczos, I. C., van de Koppel, J., & Herman, P. M. J. (2005). Trade-offs related to ecosystem engineering: A case study on stiffness of emerging macrophytes. *Ecology*, *86*(8), 2187–2199. https://doi.org/10.1890/04-1588

Bouma, T. J., van Belzen, J., Balke, T., van Dalen, J., Klaassen, P., Hartog, A. M., et al. (2016). Short-term mudflat dynamics drive long-term cyclic salt marsh dynamics. *Limnology & Oceanography*, *61*(6), 2261–2275. https://doi.org/10.1002/lno.10374

Bouma, T. J., van Belzen, J., Balke, T., Zhu, Z., Airoldi, L., Blight, A. J., et al. (2014). Identifying knowledge gaps hampering application of intertidal habitats in coastal protection: Opportunities & steps to take. *Coastal Engineering*, *87*, 147–157. https://doi.org/10.1016/j.coastaleng.2013.11.014

Callaghan, D. P., Bouma, T. J., Klaassen, P., van der Wal, D., Stive, M. J. F., & Herman, P. M. J. (2010). Hydrodynamic forcing on salt-marsh development: Distinguishing the relative importance of waves and tidal flows. *Estuarine, Coastal and Shelf Science*, *89*(1), 73–88. https://doi.org/10.1016/j.ecss.2010.05.013

Cao, H., Zhu, Z., Balke, T., Zhang, L., & Bouma, T. J. (2018). Effects of sediment disturbance regimes on Spartina seedling establishment: Implications for salt marsh creation and restoration. *Limnology & Oceanography*, *63*(2), 647–659. https://doi.org/10.1002/lno.10657

Cao, H., Zhu, Z., James, R., Herman, P. M. J., Zhang, L., Yuan, L., & Bouma, T. J. (2019). Wave effects on seedling establishment of three pioneer marsh species: Survival, morphology and biomechanics. *Annals of Botany*, *125*(2), 345–352. https://doi.org/10.1093/aob/mcz136

Chirol, C., Spencer, K. L., Carr, S. J., Möller, I., Evans, B., Lynch, J., et al. (2021). Effect of vegetation cover and sediment type on 3D subsurface structure and shear strength in saltmarshes. In *Earth surface processes and landforms*. https://doi.org/10.1002/esp.5174

Cox, R., Wadsworth, R. A., & Thomson, A. G. (2003). Long-term changes in salt marsh extent affected by channel deepening in a modified estuary. *Continental Shelf Research*, *23*(17), 1833–1846. https://doi.org/10.1016/j.csr.2003.08.002

D'Alpaos, A., & Marani, M. (2016). Reading the signatures of biologic–geomorphic feedbacks in salt-marsh landscapes. *Advances in Water Resources*, *93*, 265–275

D'Alpaos, A., Mudd, S. M., & Carniello, L. (2011). Dynamic response of marshes to perturbations in suspended sediment concentrations and rates of relative sea level rise. *Journal of Geophysical Research*, *116*(F4), F04020. https://doi.org/10.1029/2011jf002093

Damme, S. V., Struyf, E., Maris, T., Ysebaert, T., Dehairs, F., Tackx, M., et al. (2005). Spatial and temporal patterns of water quality along the estuarine salinity gradient of the Scheldt estuary (Belgium and The Netherlands): Results of an integrated monitoring approach. *Hydrobiologia*, *540*(1), 29–45. https://doi.org/10.1007/s10750-004-7102-2

De Kruif, A. C. (2001). *Bodemdieptegegevens van het Nederlandse Kustsysteem. Beschikbare digitale data en een overzicht van aanvullende analoge data* (p. 114).

de Vet, P. L. M., van Prooijen, B. C., Colosimo, I., Ysebaert, T., Herman, P. M. J., & Wang, Z. B. (2020). Sediment disposals in estuarine channels alter the eco-morphology of intertidal flats. *Journal of Geophysical Research: Earth Surface*, *125*(2), e2019JF005432. https://doi.org/10.1029/2019jf005432

Deltares (2015). *User manual DELFT3D-FLOW*. Deltares.

Deltares (2019a). *D-flow flexible Mesh user manual*.

Deltares (2019b). *D-morphology user manual*.

Deltares (2019c). *D-waves user manual*.

Doody, J. P. (2007). *Saltmarsh conservation, management and restoration*. Springer Science & Business Media.

Emanuel, K. (2005). Increasing destructiveness of tropical cyclones over the past 30years. *Nature*, *436*(7051), 686–688. https://doi.org/10.1038/nature03906

Fagherazzi, S. (2014). Coastal processes: Storm-proofing with marshes. *Nature Geoscience*, *7*(10), 701–702. https://doi.org/10.1038/ngeo2262

Feagin, R. A., Lozada-Bernard, S. M., Ravens, T. M., Möller, I., Yeager, K. M., & Baird, A. H. (2009). Does vegetation prevent wave erosion of salt marsh edges? *Proceedings of the National Academy of Sciences*, *106*(25), 10109–10113. https://doi.org/10.1073/pnas.0901297106

Francalanci, S., Bendoni, M., Rinaldi, M., & Solari, L. (2013). Ecomorphodynamic evolution of salt marshes: Experimental observations of bank retreat processes. *Geomorphology*, *195*, 53–65. https://doi.org/10.1016/j.geomorph.2013.04.026

Gedan, K. B., Kirwan, M. L., Wolanski, E., Barbier, E. B., & Silliman, B. R. (2011). The present and future role of coastal wetland vegetation in protecting shorelines: Answering recent challenges to the paradigm. *Climatic Change*, *106*(1), 7–29. https://doi.org/10.1007/s10584-010-0003-7

Hasselmann, K. F., Barnett, T. P., Bouws, E., Carlson, H., Cartwright, D. E., Eake, K., et al. (1973). Measurements of wind-wave growth and swell decay during the joint North sea wave Project (JONSWAP). In *Ergaenzungsheft zur Deutschen Hydrographischen Zeitschrift, Reihe A*.

Hu, Z., van Belzen, J., van der Wal, D., Balke, T., Wang, Z. B., Stive, M., & Bouma, T. J. (2015). Windows of opportunity for salt marsh vegetation establishment on bare tidal flats: The importance of temporal and spatial variability in hydrodynamic forcing. *Journal of Geophysical Research: Biogeosciences*, *120*(7), 1450–1469. https://doi.org/10.1002/2014jg002870

Hutton, E. W., Piper, M. D., & Tucker, G. E. (2020). The basic model Interface 2.0: A standard interface for coupling numerical models in the geosciences. *Journal of Open Source Software*, *5*(51), 2317. https://doi.org/10.21105/joss.02317

Kernkamp, H. W. J., Van Dam, A., Stelling, G. S., & de Goede, E. D. (2011). Efficient scheme for the shallow water equations on unstructured grids with application to the Continental Shelf. *Ocean Dynamics*, *61*(8), 1175–1188. https://doi.org/10.1007/s10236-011-0423-6

King, S. E., & Lester, J. N. (1995). The value of salt marsh as a sea defence. *Marine Pollution Bulletin*, *30*(3), 180–189. https://doi.org/10.1016/0025-326x(94)00173-7

Kirwan, M. L., & Guntenspergen, G. R. (2010). Influence of tidal range on the stability of coastal marshland. *Journal of Geophysical Research*, *115*(F2), F02009. https://doi.org/10.1029/2009jf001400

Kirwan, M. L., Guntenspergen, G. R., D'Alpaos, A., Morris, J. T., Mudd, S. M., & Temmerman, S. (2010). Limits on the adaptability of coastal marshes to rising sea level. *Geophysical Research Letters*, *37*(23), L23401. https://doi.org/10.1029/2010gl045489

Kirwan, M. L., & Megonigal, P. (2013). Tidal wetland stability in the face of human impacts and sea-level rise. *Nature*, *504*, 53–60. https://doi.org/10.1038/nature12856

Kirwan, M. L., & Murray, A. B. (2007). A coupled geomorphic and ecological model of tidal marsh evolution. *Proceedings of the National Academy of Sciences*, *104*(15), 6118–6122. https://doi.org/10.1073/pnas.0700958104

Kirwan, M. L., Temmerman, S., Skeehan, E. E., Guntenspergen, G. R., & Fagherazzi, S. (2016). Overestimation of marsh vulnerability to sea level rise. *Nature Climate Change*, *6*(3), 253–260. https://doi.org/10.1038/nclimate2909

Knutson, T. R., McBride, J. L., Chan, J., Emanuel, K., Holland, G., Landsea, C., et al. (2010). Tropical cyclones and climate change. *Nature Geoscience*, *3*(3), 157–163. https://doi.org/10.1038/ngeo779

Kolker, A. S., Goodbred, S. L., Hameed, S., & Cochran, J. K. (2009). High-resolution records of the response of coastal wetland systems to long-term and short-term sea-level variability. *Estuarine, Coastal and Shelf Science*, *84*(4), 493–508. https://doi.org/10.1016/j.ecss.2009.06.030

Ladd, C. J. T., Duggan-Edwards, M. F., Bouma, T. J., Pagès, J. F., & Skov, M. W. (2019). Sediment supply explains long-term and large-scale patterns in salt marsh lateral expansion and erosion. *Geophysical Research Letters*, *46*(20), 11178–11187. https://doi.org/10.1029/2019gl083315

Leckebusch, G. C., & Ulbrich, U. (2004). On the relationship between cyclones and extreme windstorm events over Europe under climate change. *Global and Planetary Change*, *44*(1), 181–193. https://doi.org/10.1016/j.gloplacha.2004.06.011

Leonardi, N., & Fagherazzi, S. (2014). How waves shape salt marshes. *Geology*, *42*(10), 887–890. https://doi.org/10.1130/g35751.1

Leonardi, N., Ganju, N. K., & Fagherazzi, S. (2016). A linear relationship between wave power and erosion determines salt-marsh resilience to violent storms and hurricanes. *Proceedings of the National Academy of Sciences*, *113*(1), 64–68. https://doi.org/10.1073/pnas.1510095112

Marani, M., D'Alpaos, A., Lanzoni, S., & Santalucia, M. (2011). Understanding and predicting wave erosion of marsh edges. *Geophysical Research Letters*, *38*(21), L21401. https://doi.org/10.1029/2011gl048995

Marijs, K. & Parée, E. (2004). Nauwkeurigheid vaklodingen Westerschelde en -monding: "de praktijk". Meetinformatiedienst Zeeland

Mariotti, G. (2020). Beyond marsh drowning: The many faces of marsh loss (and gain). *Advances in Water Resources*, *144*, 103710. https://doi.org/10.1016/j.advwatres.2020.103710

Mariotti, G., & Canestrelli, A. (2017). Long-term morphodynamics of muddy backbarrier basins: Fill in or empty out? *Water Resources Research*, *53*(8), 7029–7054. https://doi.org/10.1002/2017wr020461

Mariotti, G., & Fagherazzi, S. (2010). A numerical model for the coupled long-term evolution of salt marshes and tidal flats. *Journal of Geophysical Research*, *115*(F1), F01004. https://doi.org/10.1029/2009jf001326

Mariotti, G., & Fagherazzi, S. (2013). Critical width of tidal flats triggers marsh collapse in the absence of sea-level rise. *Proceedings of the National Academy of Sciences*, *110*(14), 5353–5356. https://doi.org/10.1073/pnas.1219600110

McLoughlin, S. M., Wiberg, P. L., Safak, I., & McGlathery, K. J. (2015). Rates and forcing of marsh edge erosion in a shallow coastal Bay. *Estuaries and Coasts*, *38*(2), 620–638. https://doi.org/10.1007/s12237-014-9841-2

Méndez, F. J., & Losada, I. J. (2004). An empirical model to estimate the propagation of random breaking and nonbreaking waves over vegetation fields. *Coastal Engineering*, *51*(2), 103–118. https://doi.org/10.1016/j.coastaleng.2003.11.003

Möller, I., Kudella, M., Rupprecht, F., Spencer, T., Paul, M., van Wesenbeeck, B. K., et al. (2014). Wave attenuation over coastal salt marshes under storm surge conditions. *Nature Geoscience*, *7*(10), 727–731. https://doi.org/10.1038/ngeo2251

Möller, I., & Spencer, T. (2002). Wave dissipation over macro-tidal saltmarshes: Effects of marsh edge typology and vegetation change. *Journal of Coastal Research*, *36*, 506–521

Mudd, S. M., Howell, S. M., & Morris, J. T. (2009). Impact of dynamic feedbacks between sedimentation, sea-level rise, and biomass production on near-surface marsh stratigraphy and carbon accumulation. *Estuarine, Coastal and Shelf Science*, *82*(3), 377–389. https://doi.org/10.1016/j.ecss.2009.01.028

Partheniades, E. (1965). Erosion and deposition of cohesive soils. *Journal of the Hydraulics Division*, *91*(1), 105–139. https://doi.org/10.1061/jyceaj.0001165

Peckham, S. D., Hutton, E. W. H., & Norris, B. (2013). A component-based approach to integrated modeling in the geosciences: The design of CSDMS. *Computers & Geosciences*, *53*, 3–12. https://doi.org/10.1016/j.cageo.2012.04.002

Pedersen, J. B. T., & Bartholdy, J. (2007). Exposed salt marsh morphodynamics: An example from the Danish Wadden Sea. *Geomorphology*, *90*(1), 115–125. https://doi.org/10.1016/j.geomorph.2007.01.012

Poppema, D. W., Willemsen, P. W. J. M., de Vries, M. B., Zhu, Z., Borsje, B. W., & Hulscher, S. J. M. H. (2019). Experiment-supported modelling of salt marsh establishment. *Ocean & Coastal Management*, *168*, 238–250. https://doi.org/10.1016/j.ocecoaman.2018.10.039

Reed, D., van Wesenbeeck, B., Herman, P. M. J., & Meselhe, E. (2018). Tidal flat-wetland systems as flood defenses: Understanding biogeomorphic controls. *Estuarine, Coastal and Shelf Science*, *213*, 269–282. https://doi.org/10.1016/j.ecss.2018.08.017

Ris, R. C., Holthuijsen, L. H., & Booij, N. (1999). A third-generation wave model for coastal regions: 2. Verification. *Journal of Geophysical Research*, *104*(C4), 7667–7681. https://doi.org/10.1029/1998jc900123

Roelvink, J. A. (2006). Coastal morphodynamic evolution techniques. *Coastal Engineering*, *53*(2), 277–287. https://doi.org/10.1016/j.coastaleng.2005.10.015

Ruessink, G., & Roelvink, J. A. (2000). *Validation of on-line mud transport within Delft3DFLOW*. WL | Delft Hydraulics

Schuerch, M., Vafeidis, A., Slawig, T., & Temmerman, S. (2013). Modeling the influence of changing storm patterns on the ability of a salt marsh to keep pace with sea level rise. *Journal of Geophysical Research: Earth Surface*, *118*(1), 84–96. https://doi.org/10.1029/2012jf002471

Schwarz, C., Gourgue, O., van Belzen, J., Zhu, Z., Bouma, T. J., van de Koppel, J., et al. (2018). Self-organization of a biogeomorphic landscape controlled by plant life-history traits. *Nature Geoscience*, *11*(9), 672–677. https://doi.org/10.1038/s41561-018-0180-y

Schwarz, C., Ye, Q. H., van der Wal, D., Zhang, L. Q., Bouma, T., Ysebaert, T., & Herman, P. M. J. (2014). Impacts of salt marsh plants on tidal channel initiation and inheritance. *Journal of Geophysical Research: Earth Surface*, *119*(2), 385–400. https://doi.org/10.1002/2013jf002900

Schwimmer, R. (2001). Rates and Processes of Marsh Shoreline Erosion in Rehoboth Bay, Delaware, U.S.A. *Journal of Coastal Research*, *17*, 672–683

Shepard, C. C., Crain, C. M., & Beck, M. W. (2011). The Protective Role of Coastal Marshes: A Systematic Review and Meta-analysis. *PLoS One*, *6*(11), e27374. https://doi.org/10.1371/journal.pone.0027374

Siemes, R., Borsje, B. W., Daggenvoorde, R., & Hulscher, S. (2020). Artificial structures steer morphological development of salt marshes: A model study. *Journal of Marine Science and Engineering*, *8*, 326. https://doi.org/10.3390/jmse8050326

Silinski, A., van Belzen, J., Fransen, E., Bouma, T. J., Troch, P., Meire, P., & Temmerman, S. (2016). Quantifying critical conditions for seaward expansion of tidal marshes: A transplantation experiment. *Estuarine, Coastal and Shelf Science*, *169*, 227–237. https://doi.org/10.1016/j.ecss.2015.12.012

Singh Chauhan, P. P. (2009). Autocyclic erosion in tidal marshes. *Geomorphology*, *110*(3), 45–57. https://doi.org/10.1016/j.geomorph.2009.03.016

Soetaert, K., Petzoldt, T., & Setzer, R. (2010). Solving differential equations in R: Package deSolve. *Journal of Statistical Software*, *33*, 1–25. https://doi.org/10.18637/jss.v033.i09

Stecca, G., Measures, R., & Hicks, D. M. (2017). A framework for the analysis of noncohesive bank erosion algorithms in morphodynamic modeling. *Water Resources Research*, *53*(8), 6663–6686. https://doi.org/10.1002/2017wr020756

Suzuki, T., & Arikawa, T. (2010). *Numerical analysis of bulk drag coefficient in dense vegetation by immersed boundary method*.

Suzuki, T., Zijlema, M., Burger, B., Meijer, M. C., & Narayan, S. (2012). Wave dissipation by vegetation with layer schematization in SWAN. *Coastal Engineering*, *59*(1), 64–71. https://doi.org/10.1016/j.coastaleng.2011.07.006

Tambroni, N., & Seminara, G. (2012). A one-dimensional eco-geomorphic model of marsh response to sea level rise: Wind effects, dynamics of the marsh border and equilibrium. *Journal of Geophysical Research*, *117*(F3), F03026. https://doi.org/10.1029/2012jf002363

Temmerman, S., Bouma, T. J., Govers, G., Wang, Z. B., De Vries, M. B., & Herman, P. M. J. (2005). Impact of vegetation on flow routing and sedimentation patterns: Three-dimensional modeling for a tidal marsh. *Journal of Geophysical Research*, *110*(F4), F04019. https://doi.org/10.1029/2005jf000301

Temmerman, S., Bouma, T. J., Van de Koppel, J., Van der Wal, D., De Vries, M. B., & Herman, P. M. J. (2007). Vegetation causes channel erosion in a tidal landscape. *Geology*, *35*(7), 631–634. https://doi.org/10.1130/g23502a.1

Temmerman, S., Govers, G., Wartel, S., & Meire, P. (2004). Modelling estuarine variations in tidal marsh sedimentation: Response to changing sea level and suspended sediment concentrations. *Marine Geology*, *212*(1), 1–19. https://doi.org/10.1016/j.margeo.2004.10.021

Temmerman, S., Meire, P., Bouma, T. J., Herman, P. M. J., Ysebaert, T., & De Vriend, H. J. (2013). Ecosystem-based coastal defence in the face of global change. *Nature*, *504*(7478), 79–83. https://doi.org/10.1038/nature12859

Tonelli, M., Fagherazzi, S., & Petti, M. (2010). Modeling wave impact on salt marsh boundaries. *Journal of Geophysical Research*, *115*(C9), C09028. https://doi.org/10.1029/2009jc006026

Turner, R. E., Swenson, E. M., Milan, C. S., Lee, J. M., & Oswald, T. A. (2004). Below-ground biomass in healthy and impaired salt marshes. *Ecological Research*, *19*(1), 29–35. https://doi.org/10.1111/j.1440-1703.2003.00610.x

Van Damme, S., Ysebaert, T., Meire, P., & Van den Berg, E. (1999). *Habitatstructuren, waterkwaliteit en leefgemeenschappen in het Schelde-estuarium*. Instituut voor Natuurbehoud, 99/24

Van de Koppel, J., Van der Wal, D., Bakker, J. P., & Herman, P. M. J. (2005). Self-Organization and Vegetation Collapse in Salt Marsh Ecosystems. *The American Naturalist*, *165*(1), E1–E12. https://doi.org/10.1086/426602

Van der Wal, D., Wielemaker-Van den Dool, A., & Herman, P. M. J. (2008). Spatial patterns, rates and mechanisms of saltmarsh cycles (Westerschelde, The Netherlands). *Estuarine, Coastal and Shelf Science*, *76*(2), 357–368. https://doi.org/10.1016/j.ecss.2007.07.017

van Hulzen, J. B., van Soelen, J., & Bouma, T. J. (2007). Morphological variation and habitat modification are strongly correlated for the autogenic ecosystem engineer Spartina anglica (common cordgrass). *Estuaries and Coasts*, *30*(1), 3–11. https://doi.org/10.1007/bf02782962

van Veelen, T. J., Fairchild, T. P., Reeve, D. E., & Karunarathna, H. (2020). Experimental study on vegetation flexibility as control parameter for wave damping and velocity structure. *Coastal Engineering*, *157*, 103648. https://doi.org/10.1016/j.coastaleng.2020.103648

Vuik, V., Borsje, B. W., Willemsen, P. W. J. M., & Jonkman, S. N. (2019). Salt marshes for flood risk reduction: Quantifying long-term effectiveness and life-cycle costs. *Ocean & Coastal Management*, *171*, 96–110. https://doi.org/10.1016/j.ocecoaman.2019.01.010

Vuik, V., Jonkman, S. N., Borsje, B. W., & Suzuki, T. (2016). Nature-based flood protection: The efficiency of vegetated foreshores for reducing wave loads on coastal dikes. *Coastal Engineering*, *116*, 42–56. https://doi.org/10.1016/j.coastaleng.2016.06.001

Wamsley, T. V., Cialone, M. A., Smith, J. M., Atkinson, J. H., & Rosati, J. D. (2010). The potential of wetlands in reducing storm surge. *Ocean Engineering*, *37*(1), 59–68. https://doi.org/10.1016/j.oceaneng.2009.07.018

Wang, H., van der Wal, D., Li, X., van Belzen, J., Herman, P. M. J., Hu, Z., et al. (2017). Zooming in and out: Scale dependence of extrinsic and intrinsic factors affecting salt marsh erosion. *Journal of Geophysical Research: Earth Surface*, *122*(7), 1455–1470. https://doi.org/10.1002/2016jf004193

Wiegman, N., Perluka, R., Oude Elberink, S., & Vogelzang, J. (2005). *Vaklodingen: De inwintechnieken en hun combinaties. Vergelijking tussen verschillende inwintechnieken en de combinaties ervan* (p. 47).

Willemsen, P. W. J. M., Borsje, B. W., Hulscher, S. J. M. H., Van der Wal, D., Zhu, Z., Oteman, B., et al. (2018). Quantifying bed level change at the transition of tidal flat and salt marsh: Can we understand the lateral location of the marsh edge? *Journal of Geophysical Research: Earth Surface*, *123*(10), 2509–2524. https://doi.org/10.1029/2018jf004742

Willemsen, P. W. J. M., Borsje, B. W., Vuik, V., Bouma, T. J., & Hulscher, S. J. M. H. (2020). Field-based decadal wave attenuating capacity of combined tidal flats and salt marshes. *Coastal Engineering*, *156*, 103628. https://doi.org/10.1016/j.coastaleng.2019.103628

Zhang, R. S., Shen, Y. M., Lu, L. Y., Yan, S. G., Wang, Y. H., Li, J. L., & Zhang, Z. L. (2004). Formation of Spartina alterniflora salt marshes on the coast of Jiangsu Province, China. *Ecological Engineering*, *23*(2), 95–105. https://doi.org/10.1016/j.ecoleng.2004.07.007

Zhang, W., Zeng, C., Tong, C., Zhang, Z., & Huang, J. (2011). Analysis of the expanding process of the Spartina Alterniflora salt marsh in Shanyutan Wetland, Minjiang River Estuary by remote sensing. *Procedia Environmental Sciences*, *10*, 2472–2477. https://doi.org/10.1016/j.proenv.2011.09.385

Zhang, X., Xiao, X., Wang, X., Xu, X., Chen, B., Wang, J., et al. (2020). Quantifying expansion and removal of Spartina alterniflora on Chongming island, China, using time series Landsat images during 1995–2018. *Remote Sensing of Environment*, *247*, 111916. https://doi.org/10.1016/j.rse.2020.111916

Zhao, Y., Yu, Q., Wang, D., Wang, Y. P., Wang, Y., & Gao, S. (2017). Rapid formation of marsh-edge cliffs, Jiangsu coast, China. *Marine Geology*, *385*, 260–273. https://doi.org/10.1016/j.margeo.2017.02.001

Zhu, Z., van Belzen, J., Zhu, Q., van de Koppel, J., & Bouma, T. J. (2020). Vegetation recovery on neighboring tidal flats forms an Achilles' heel of saltmarsh resilience to sea level rise. *Limnology & Oceanography*, *65*(1), 51–62. https://doi.org/10.1002/lno.11249

Zhu, Z., Vuik, V., Visser, P. J., Soens, T., van Wesenbeeck, B., van de Koppel, J., et al. (2020). Historic storms and the hidden value of coastal wetlands for nature-based flood defence. *Nature Sustainability*, *3*, 853–862. https://doi.org/10.1038/s41893-020-0556-z